# University of Alberta

The Physical and Geochemical Characteristics of Diamonds from the Artemisia Kimberlite (Northern Slave Craton, Nunavut, Canada)

*AND*

The Micro-/Macro-Diamond Relationship

by

Catherine Nadine Johnson

A thesis submitted to the Faculty of Graduate Studies and Research
in partial fulfillment of the requirements for the degree of

Master of Science

Department of Earth and Atmospheric Sciences



Fall 2011

Edmonton, Alberta

## Abstract

This thesis presents the results of a study on diamonds from the Artemisia kimberlite, Nunavut, Canada. This study integrates the isotopic, chemical and physical characteristics of the diamonds in an attempt to provide insight into the nature of the micro-/macro-diamond genetic relationship, and its possible implication pertaining to the use of size frequency distributions in modern kimberlite exploration programs.

Despite geochemical commonalities of the Artemisia micro- and macro-diamonds, distinct signatures are observed, particularly in regards to enriched and depleted carbon isotopic compositions, the abundance of nitrogen and hydrogen impurities and different resorption histories. This implies that, despite an observed lognormal size frequency distribution for Artemisia diamonds, micro- and macro-diamonds do not represent a single population at this locality.

## Acknowledgements

First of all, I would like to thank my supervisor Thomas Stachel for encouraging me to pursue graduate studies and introducing me to kimberlites, cratons and diamonds. Without his support, enthusiasm and encouragement, my time with the Diamond Research Group would have not been quite as enjoyable.

I am especially grateful to Tom McCandless for initiating this project.

I would like to thank John Armstrong and Stornoway Diamond Corp. for providing me with the samples I used for this project.

Thank you Karlis Muehlenbachs for your enthusiasm, helpful comments and limitless access to your lab.

I would like to thank staff at the Edinburgh Ion Microprobe Facility for all their help and assistance. A big thank you especially to John Craven, for his restaurant recommendations and introducing me to the delights of Friday afternoon beverages.

Thank you to Richard Stern and the staff at the Canadian Centre for Isotopic Microanalysis for his helpful discussions and their help with sample preparation and assistance with analyzes.

I would like to thank the past and present members of the DRG, Lucy Hunt and Greg Melton in particular, for countless enlightening discussions, lab assistance and emotional support.

# Table of Contents

## Table of Contents cont.

## List of Tables

## List of Figures

## List of Symbols and Abbreviations

| | |
|---|---|
| Ga | billion years |
| Ma | million years |
| FTIR | Fourier Transform Infrared |
| V-PDB | Vienna Pee-Dee Belemnite |
| SIMS | secondary ion mass spectrometry |
| MC-SIMS | multi-collection secondary ion mass spectrometry |
| ppm | parts per million |
| ‰ | per mil |
| at.ppm | atomic parts per million |
| wt.ppm | weight parts per million |
| $T_N$ | time averaged residence temperature |
| $N_T$ | total nitrogen content |
| $N_B$ | nitrogen as B-center |
| $N_{ppm}$ | parts per million nitrogen |
| I(B') | platelet peak intensity |
| %B | percentage of nitrogen in B-center |
| EIMF | Edinburgh Ion Microprobe Facility |
| CCIM | Canadian Centre for Isotopic Microanalysis |
| EM | electron multiplier |
| CL | cathodoluminescence |

**From Tables**

| | |
|---|---|
| Agg | aggregate |
| (frag) | fragment |
| O | octahedron |
| M | macle |
| D | dodecahedroid |
| | |
| c | colourless |
| vlb | very light brown |
| lb | light brown |
| b | brown |
| lpb | light pink-brown |
| pb | pink-brown |
| dpb | deep pink-brown |
| ly | light yellow |
| y | yellow |
| P.D. | plastic deformation |
| bd | below the limit of detection |
| nd | not determined |

# Chapter 1

# Introduction

## 1.1. Introduction

Diamond is highly sought after not only for its value as a gemstone but also for its unique mineral properties. For example, being the hardest mineral known, diamond is used in industrial applications such as drilling, cutting and polishing.

The majority of natural diamonds are formed at depths ~150 to 200km within cool lithospheric mantle, beneath blocks of ancient, stable continental crust called cratons. Diamond is transported to the Earth's surface in deep rooted kimberlite and lamproite magmas as xenocrysts.

In Canada, the term macro-diamond is applied to all diamonds in excess of 0.5mm in size. Diamond is a trace component in kimberlite/lamproite and, as a result, grade evaluation during advanced exploration and feasibility studies requires costly bulk sampling of several thousand tons of ore. As there is a much greater abundance of micro-diamonds compared to economic macro-diamonds, the study of micro-diamonds as a predictive tool for grade distribution is economically favourable. Samples submitted for micro-diamond testing through caustic fusion usually are in the order of kilograms.

First studied by Deakin and Boxer (1989) on diamonds from Argyle mine (Western Australia), it was recognized that, on a log-log plot, the frequency of micro-diamonds (number of stones per ton of kimberlite) and the sieve class (nominal aperture size in mm) display a near-linear correlation, which can be extrapolated to predict the macro-diamond grade of a kimberlite. The application of this technique assumes representative sampling of micro-diamonds.

Although not relevant for the statistical validity of the methodology (Chapman and Boxer, 2004), the observation of lognormal size frequency distributions appears to imply that micro- and macro-diamonds are derived from common sources. However, this implication of co-genesis has not yet been conclusively studied. To resolve this question, the carbon isotopic compositions and nitrogen characteristics of diamonds from the Artemisia kimberlite, Northern Slave, displaying a lognormal size frequency distribution (Figure 1.1), were studied to determine if a source commonality is reflected in the micro- and macro-diamonds.

## 1.2. The Slave Craton and the Artemisia Kimberlite

The Artemisia kimberlite was discovered in 2001 by Ashton Mining of Canada Inc. and is located in the Coronation Gulf diamond district of the Northern Slave craton (as defined by Grütter et al., 1999; see Figure 1.2). The pipe intrudes sediments of the Coronation Supergroup, a shelf-rise sedimentary sequence deposited just prior to the Wopmay orogeny (1.9Ga). The kimberlite was found to outcrop at the head of a well defined indicator mineral train. Drilling in 2002 confirmed that Artemisia is a vent-like body estimated to be approximately 3ha in size (Ward and Clements, 2002). Although the age of Artemisia has yet to be determined, another kimberlite nearby, Anuri, has been dated to ~613±6Ma (Masun et al., 2004), and this age is assumed to apply to Artemisia as well.

The Slave is a small late Archean craton located in northwest of the Canadian Shield (Hoffman, 1988). The Slave Craton is bounded by Proterozoic orogenes to the east (Taltson-Thelon) and west (Wopmay), both of which formed during the amalgamation of Laurentia ca. 2.0-1.8Ga (Hoffman, 1988). The Slave craton is subdivided into three north-east trending domains based on compositional differences derived via the $Cr_2O_3$-CaO compositions of peridotitic garnets (manly from till samples) reflecting variations in the extent of depletion of the underlying lithospheric mantle (Grütter et al. 1999).The Wopmay orogen developed during the Calderain orogeny, occurring 1.92 to 1.84 Ga (Hoffman, 1988). The Calderain orogeny thrust the Coronation Supergroup onto the Slave Craton and amalgamated the Hottah and Fort Simpson terranes onto its western margin. The Coronation Supergroup is broadly described as a passive margin and fore-deep succession comprised of turbidites, arenites, calcareous argillites and shales (e.g. Ward and Clements, 2002) and consists of three groups: (1) The Melville, a rift facies assemblage consisting of volcanic and coarse grained clastic rocks (Hoffman and Pelletier, 1982); (2) The Epworth, a shallow marine sequence representing a west-facing passive margin (Hoffman, 1973); (3) The Recluse, a collision related fore-deep assemblage (Hoffman, 1973). The Coronation Supergroup is intruded by the Morel sills, a syncollisional suite of north-trending gabbroic intrusives (Hoffman, 1987) interpreted to be the result of the ‘failed’ subduction of the Slave craton beneath the Hottah terrane (Hildebrand and Bowring, 1999).

Subsequent to the Wopmay orogen, the northwest Slave Craton became host to the ~1270Ma Mackenzie large igneous province (LeCheminant and

Heaman, 1989). The Mackenzie large igneous province is characterized as a short-lived, massive event which was occurred over the presence of a large mantle plume. The resulting magmatism is associated with the Mackenzie dyke swarm, the Coppermine flood basalts and the Muskcox layered intrusion (LeCheminant and Heaman, 1989).

### 1.3. Carbon Isotopic Composition and Nitrogen Characteristics of Diamond

Determining the carbon isotopic composition ($\delta^{13}C$) of diamond has become a standard tool in diamond studies aiming to determine mechanisms of diamond formation in the Earth's mantle. The $\delta^{13}C$ of diamond is, to some extent, dependent on the $\delta^{13}C$ value of the diamond source. As a result, there are broad correlations between $\delta^{13}C$ of diamond and source paragenesis. Peridotitic diamonds, assumed to be derived from mantle carbon (Deines, 1980; Cartigny, 2005), typically display a narrow range in $\delta^{13}C$ values (-10 to -2‰; Kirkley et al., 1991; Cartigny et al., 1998a,b) about a mode at -5‰ (the assumed mantle value). Eclogitic diamonds, on a worldwide scale, display a similar mode about the mantle carbon isotopic value, but show a much wider range and a characteristic tail to highly $^{13}C$ depleted values with $\delta^{13}C$ varying from -41‰ (De Stefano et al., 2009) to +3‰ (Davies et al.., 2003). Eclogitic diamonds with light carbon isotopic compositions are often attributed to derivation from graphitized organic matter contained in subducted oceanic crust (Sobolev and Sobolev, 1980; Kirkley et al., 1991; McCandless and Gurney, 1997).

Nitrogen is the most common impurity in diamond (Kaiser and Bond, 1959). Nitrogen abundance in diamond is either controlled by kinetic factors during growth (e.g., Cartigny et al., 2001) or depends on the nitrogen concentration in the diamond growth medium (e.g., Stachel et al., 2009). For a given nitrogen abundance, the degree of nitrogen aggregation in diamond - i.e. the transition from originally single substitutional nitrogen atoms to pairs of nitrogen atoms and, finally, to rings of four nitrogen atoms surrounding a vacancy (Evans et al., 1981) - is dependent upon mantle residence time and temperature (Evans and Harris, 1989; Taylor et al., 1990). For an assumed mantle residence time, the nitrogen abundance and aggregation of a diamond can be used to calculate time averaged residence temperatures (Taylor et al., 1990; Leahy and Taylor, 1997), which, based on assumed steady state geotherms, can then be associated with depths of origin.

Many studies have been conducted on diamonds from the Slave Craton

which included isotopic analysis covering the Lac de Gras kimberlite field in the Central Slave (eg. Davies et al., 1999 and 2004; Donnelly et al., 2007; Cartigny et al., 2009), the Jericho kimberlite in the Northern Slave (De Stefano et al., 2009) and the Snap Lake kimberlite in the Southern Slave Province (Pokhilenko et al., 2004). These previous studies illustrate that variability in the source of diamond carbon exists in the lithospheric mantle underlying the Slave Craton.

Employing these two parameters pertaining to diamond source and mantle residence ($\delta^{13}C$ and N characteristics) and applying them to micro- and macro-diamonds from the same kimberlite will illustrate the nature of their genetic relationship and, in addition, will provide insights into the thermal evolution of the lithospheric mantle beneath the Northern Slave. The analytical procedures and parameters used to determined the carbon stable isotopic compositions and nitrogen characteristics of the Artemisia diamonds are described in detail in the proceeding chapter and Appendix A.

## References

Bleeker, W., Hall, B. 2007. The Slave Craton; geology and metallogenic evolution, In: Goodfellow, W.D. (ed.), Mineral Deposits of Canada: A Synthesis of Major Deposit Types, District Metallogency, The Evolution of Geological Provinces and Exploration Methods: Geological Association of Canada, Mineral Deposits Division, Special Publication No. 5, pp.849-879

Cartigny, P. 2005. Stable isotopes and the origin of diamonds. Elements 1(2):79-85

Cartigny, P., Harris, J.W., Javoy, M. 1998a. Eclogitic diamond formation at Jwangeng: no room for recycled component. Science 280 (5368): 1421-1424

Cartigny, P. Harris, J.W., Philips, D. Girard, M., Javoy, M. 1998b. Subduction related diamonds? The evidence from a mantle-derived origin from coupled $\delta^{13}C$-$\delta^{15}N$ determinations. Chemical Geology 147 (1-2): 147-159

Cartigny, P., Harris, J.W., Javoy, M. 2001. Diamond genesis, mantle fractionations and mantle nitrogen content: a study of $\delta^{13}C$-N concentrations in diamonds. Earth and Planetary Science Letters 185: 85-98

Chapman, J.G., Boxer, G.L. 2004. Size frequency distribution analyses for estimating diamond grade and value. Lithos 76: 369-375

Davies,R.M.,Griffin, W.L., Pearson, N.J., Andrew, A.S., Doyle, B.J., O'Reilly, S.Y. 1999. Diamonds from the deep: pipe DO27, Slave Craton, Canada, In: Gurney, J.J., Gurney, J.L., Pascoe, M.D., Richardson, S.H. (eds), The J.B.Dawson Volume, Proceedings of the VIIth International Kimberlite Conference. Red Roof Design, CapeTown, pp.148-155

Davies, RM., Griffin, W.L., O'Reilly, S.Y., Andrew, A.S. 2003. Unusual mineral inclusions and carbon isotopes of alluvial diamonds from Bingara, eastern Australia. Lithos 69(1-2):51-66

Davies, R.M., Griffin, W.L., O'Reilly, S.Y., Doyle,B.J. 2004. Mineral inclusions and geochemical characteristics of micro-diamonds from the DO27, A154, A21, A418, DO18, DD17 and Ranch Lake kimberlites at Lac de Gras, Slave Craton, Canada. Lithos 77:39-55

Deakin, A.S., Boxer, G.L. 1989. Argyle AK1 diamond size distributions: the use of fine diamonds to predict the occurrence of commercial sized diamonds. In: Ross, J., Jaques, A.L., Ferguson, J., Green, D.H., O'Reilly, S.Y., Danchin, R.V., Janse, A.J.A. (eds.) Kimberlites and Related Rocks, Geological Society of Australia, Special Publication Vol.14, Blackwell Carlton (1989), pp.1117-1122

Deines, P. 1980. The carbon isotopic composition of diamonds: relationship to diamond shape, colour, occurrence and vapour composition. Geochimica et Cosmochimica Acta 44(1): 943-961

De Stefano, A., Kopylova, M.G., Cartigny, P., Afanasiev, V. 2009. Diamonds and eclogites of the Jericho kimberlite (Northern Canada). Contributions to Mineralogy and Petrology 158(3):295-315

Donnelly, C.L., Stachel, T., Creighton, S., Muehlenbachs, K., Whiteford, S..2007. Diamonds and their mineral inclusions from the A154 South pipe, Diavik Diamond Mine, Northwest Territories, Canada. Lithos 98(1):160-176

Evans, T., Qi, Z., Maguire, J. 1981. The stages of nitrogen aggregation in diamond. Journal of Physics C: Solid State Physics 14(12):L379-L384

Evans, T., Harris, J.W., 1989. Nitrogen aggregation, inclusion equilibration temperatures and the age of diamonds. In: Ross J., Jaques, A.L., Ferguson, J., Green, D.H., O'Reilly, S.Y., Danchin, R.V., Janse, A.J.A. (eds.) Kimberlite and Related Rocks, Geological Society of Australia, Special Publication Vol. 14, Blackwell and Carlton (1989), pp. 1001-1006

Grütter, H.S., Apter, D.B., Kong, J. 1999. Crust-mantle coupling:evidence from mantle derived xenocrystic garnets. In: Gurney, J.J., Gurney, J.L., Pascoe, M.D., Richardson, S.H. (eds), The J.B.Dawson Volume, Proceedings of the VIIth International Kimberlite Conference. Red Roof Design, Cape Town, pp.307-313

Hildebrand, R.S., Bowring, S.A. 1999. Crustal recycling by slab failure. Geology 27(1):11-14

Hoffman, P. 1973. Evolution of an Early Proterozoic continental margin: The Coronation Geosyncline and associated aulacogens of the Northwestern Canadian Shield.Philosophical Transactions of the Royal Society of London Series A 273(1235):547-581

Hoffman, P.F. 1988. United plates of America, the birth of a craton: Early Proterozoic assembly and growth of Laurentia. Annual Reviews of Earth and Planetary Science Letters 16:543-603

Hoffman, P.F., Pelletier, K.S. 1982. Cloos nappe in Wopmay orogen: significance for stratigraphy of the Akaicho group, and implications for opening and closing of an early Proterozoic continental margin. Geological Survey of Canada, Paper 82-1A, pp.109-115

Kaiser, W. Bond, W.L. 1959. Nitrogen, a major impurity in common type I diamond. Physical Review 115(4):857-863

Kirkley, M.B., Gurney, J.J., Otter, M.L., Hill, S.J., Daniels, L.R. 1991. The application of C isotope measurements to the identification of sources of C in diamonds: a review. Applied Geochemistry 6:477-494

LeCheminant, A.N., Heaman, L.M. 1989. Mackenzie igneous events, Canada: Middle Proterozoic magmatism associated with ocean opening. Earth and Planetary Science Letters 96: 38-48

Leahy, K., Taylor, W.R. 1997. The influence of the Glennie domain deep structure on diamonds in Saskatchewan kimberlites. Russian Geology and Geophysics 38(2): 481-491

Masun, K.M.,Doyle,B.J.,Ball,S.,Walker,S.2004.The geology and mineralogy of the Anuri kimberlite, Nunavut, Canada. Lithos 76(1-4):75-97

McCandless, T.E., Gurney, J.J.1997. Diamond eclogites: comparison with carbonaceous chondrites, carbonaceous shales, and microbial carbon enriched MORB. Russian Geology and Geophysics 38(2):371-381

Pokhilenko, N.P., Sobolev, N.V. Reutsky, V.N., Hall, A.E., Taylor, L.A.2004. Crystalline inclusions and C isotope ratios in diamonds from the Snap Lake/King Lake kimberlite dyke system: evidence of ultra deep and enriched lithospheric mantle. Lithos 77:57-67

Sobolev, V.S., Sobolev, N.V. 1980. New proof on very deep subsidence of eclogitized crustal rocks. Doklady Akademii Nauk SSSR 250:683-685

Stachel, T., Harris, J.W., Muehlenbachs, K. 2009.Sources of carbon in inclusion bearing diamonds. Lithos 112(S2):625-637

Taylor, W.R., Jaques, A.L., Ridd, M.1980.Nitrogen-defect aggregation characteristics of some Australasian diamonds: time-temperature constraints on the source regions of pipe and alluvial diamonds. American Mineralogist 75:1290-1310

Ward, J.,Clements, B.2002.Technical report and recommendations, Northern Slave Properties, Nunavut., Ashton Mining of Canada Inc, 57pp.

## Figures

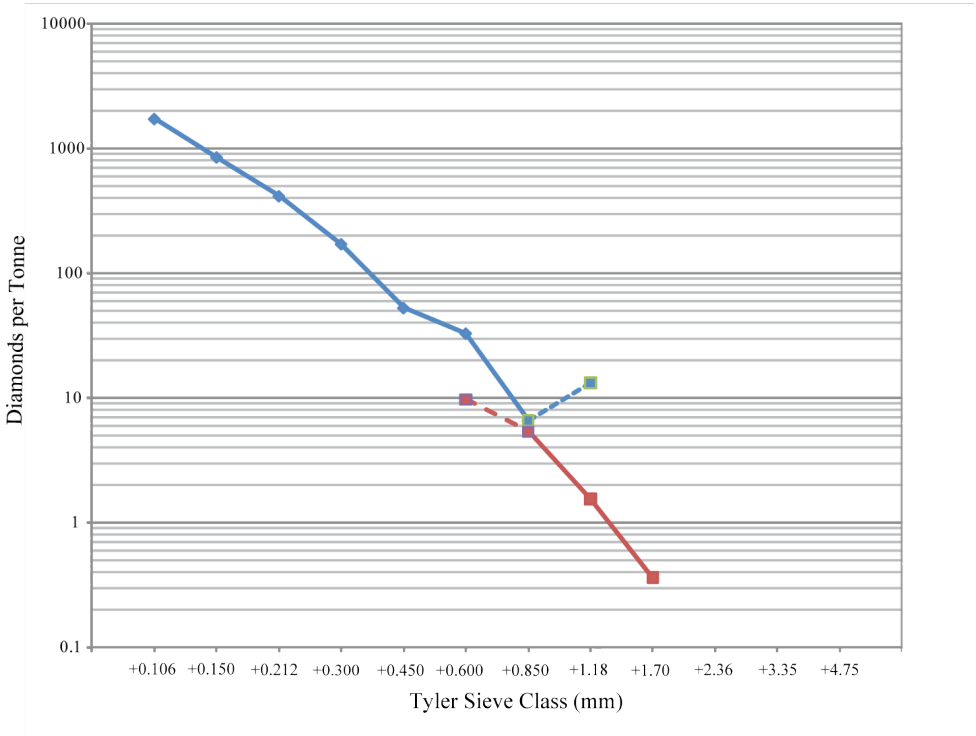


**Figure 1.1.** Size frequency distribution for the Artemisia Kimberlite. The blue line represents (main micro-) diamonds retrieved from a 151.7kg kimberlite sample processed by caustic fusion; the red line represents (mainly macro-) diamonds retrieved from an 11t kimberlite bulk sample processed by dense media separation. Dashed lines indicate non-representative sampling for small ('nugget effect') and large ('kick back') size diamonds for respective processing method. Previously unpublished data supplied by Stornoway Diamond Corp.

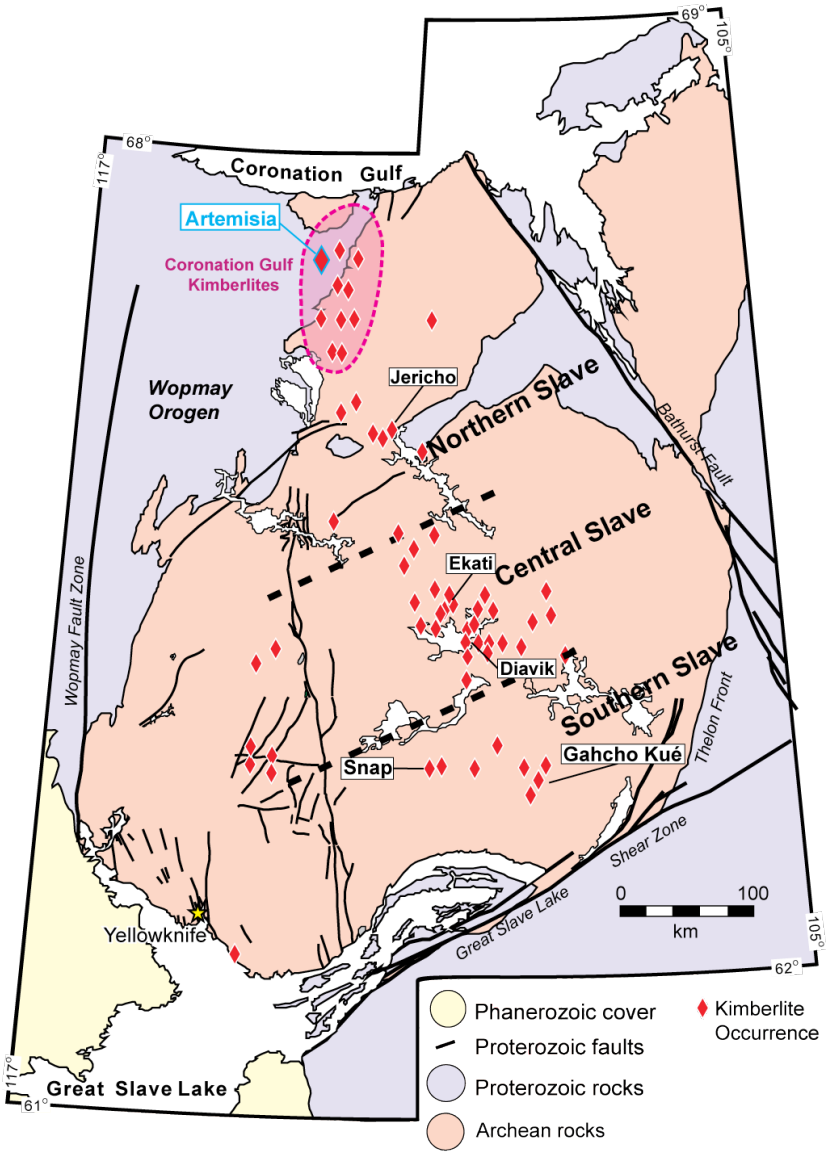


**Figure 1.2.** Map of the Slave Craton, illustrating major domains and kimberlite occurrences. Modified from Bleeker and Hall (2007).

# Chapter 2

## The Micro-/Macro-Diamond Relationship: A Case Study from the Artemisia Kimberlite (Northern Slave Craton, Canada)

The content of this chapter is in preparation to be submitted for publication as:
**The Micro-/Macro-Diamond Relationship: A Case Study on the Artemisia Kimberlite (Northern Slave Craton, Canada)**
Johnson, C.N., Stachel, T., Muehlenbachs, K., Stern, R., Edinburgh Ion Microprobe Facility (EIMF), Armstrong, J.

## 2.1. Introduction

### 2.1.1 Background

Size frequency distribution analyses have become a standard tool in modern kimberlite exploration. Important economic decisions relating to diamond grade and mining feasibility rely upon the extrapolation of micro-diamond size frequency distributions to predict the macro-diamond grade of a kimberlite (Chapman and Boxer, 2004). First recognized by Deakin and Boxer (1989) for the Argyle diamond mine (Western Australia), the frequency of stones per ton of kimberlite and the mean stone size (e.g. sieve size in mm) commonly display a near linear relationship on a log-log plot. The application of this technique to predict macro-diamond grade requires complete sampling of the micro-diamond in-situ size distribution (no loss during caustic fusion or acid digestion).

The observation of lognormal size distributions suggests a common origin of micro- and macro-diamonds. Such a genetic relationship has, however, never been conclusively established. Whilst some previous studies supported the view that micro-diamonds represent an extension of the macro population to smaller stone sizes (e.g. McCandless et al., 1994), others , based on morphology (Pattison and Levinson, 1995) and mineral inclusion content (Sobolev et al., 2004), suggested that micro-diamonds reflect, at least in part, distinct diamond forming events or mantle sources. Although a genetic relationship between micro- and macro-diamonds may not be important for practical application (Chapman and

Boxer, 2004), validating or disproving such a relationship will elucidate the empirical observation of log normal size distributions from a process point of view.

Geochemical studies on diamond provide insights into the isotopic (Deines, 1980; Cartigny, 2001) and compositional (e.g. Araujo et al., 2008; McNeill et al., 2009) characteristics of its sources in the lithospheric upper mantle. In particular, the carbon stable isotopic composition and the abundance and aggregation state of nitrogen have been used to determine the origin and residence history of diamond within the mantle. The carbon isotopic composition of diamond depends upon the carbon isotopic composition of its growth medium and, consequently, shows some relationship to source paragenesis. Peridotitic diamonds, assumed to derive from mantle carbon (e.g., Deines, 1980; Cartigny, 2005), typically display a narrow range in carbon isotopic composition ($\delta^{13}C$) with a mode about -5‰. On a worldwide scale, eclogitic diamonds, for which carbon may partially be sourced in subducted oceanic crust (Sobolev and Sobolev, 1980; Kirkley et al., 1991; McCandless and Gurney, 1997), display a similar mode in carbon isotopic composition to peridotitic diamonds, though their distribution is distinctly skewed to lighter isotopic compositions. The worldwide data base for eclogitic diamonds is, however, strongly biased through an overabundance of analyses from the Kalahari Craton and the prominent mode ~-5‰ observed there does not exist among eclogitic diamonds from e.g. the Amazon and Kimberley cratons (Stachel et al., 2009). The abundance of nitrogen in diamond may either depend on the nitrogen concentration in the diamond growth medium (e.g. Stachel et al. 2009) or may be controlled by kinetic factors during growth (e.g. Cartigny et al., 2001). For a given nitrogen abundance, the degree of nitrogen aggregation depends upon mantle residence time and temperature (Evans and Harris, 1989;

Taylor et al., 1990; Leahy and Taylor, 1997). In consequence, analysing the carbon isotopic composition, the nitrogen content and the nitrogen aggregations state of micro- and macro-diamonds from the same kimberlite in conjunction, will allow us to examine whether their relationship is co-genetic or not.

### 2.1.2 Artemisia Kimberlite

Discovered in 2001 by Ashton Mining of Canada (now dissolved into Stornoway Diamond Corporation), the diamondiferous Artemisia kimberlite is located in the Coronation Bay diamond district of the Northern Slave Craton (as defined by Grütter et al., 1999). The Artemisia pipe is situated along the western margin of the craton (Figure 2.1). The kimberlite intrudes sediments of the Protoerozoic Coronation Supergroup, a shelf-rise sedimentary sequence composed of calcareous argillites, arenites, shales and turbidites deposited during the 1.9Ga Wopmay orogeny, a collisional event which accreted the Hottah terrane onto the western margin of the Slave Craton (Hoffman, 1988) and led to the subduction related magmatism associated with the formation of the Great Bear magmatic zone (Hildebrand et al., 1987). The Coronation Supergroup was subsequently compressed and thrust eastward onto the Slave Craton. During the collision, the Coronation Supergroup was intruded by the Morel sills, a suite of north trending gabbroic intrusions (Hoffman, 1987).

An emplacement age for Artemisia itself is not available, but the nearby Anuri kimberlite has been dated to ~613±6 Ma (Masun et al., 2004) and an Eocambrian age may hence apply to Artemisia as well. Artemisia has been characterized as a diatreme facies kimberlite and is approximately 3ha in size (Ward and Clements, 2002).

## 2.2. Analytical Methods

We selected 209 diamonds from a total of 961 diamonds recovered from the Artemisia kimberlite by bulk sampling. The selected diamonds range in size from 0.106mm to 1.70mm in Tyler sieve class (lower aperture) and have been characterized for their morphology, colour, evidence for plastic deformation and surface features as summarized in Table 2.1. Samples ≤0.5mm in size are denoted as micro-diamonds.

Nitrogen abundances and aggregation states were determined at the University of Alberta using a Thermo-Nicolet Fourier Transform Infrared (FTIR) spectrometer coupled with a Continuum microscope with a KBr splitter. Methods and procedures were the same as described in Banas et al. (2007). Deconvolution of spectra to determine nitrogen abundances and aggregation states was achieved using software provided by David Fisher (Research Laboratories of the Diamond Trading Company, Maidenhead, UK). Nitrogen concentrations (in atomic ppm) were calculated from absorption coefficient values at 1282$cm^{-1}$ for both nitrogen A-centers (Boyd et al., 1994) and B-centers (Boyd et al., 1995). Typical detection limits range from 5 to 15 atomic ppm with an analytical precision about 5-10% of the measured nitrogen abundance.

The carbon isotopic compositions of the 108 macro-diamonds were measured using a conventional sealed tube combustion technique and subsequent mass spectrometry (dual inlet Finnigan Mat 252) at the University of Alberta, with an analytical precision of ± 0.05‰; results are reported relative to V-PDB standard. Whole stones and fragments with masses between 0.4-2.0mg were combusted at 980˚C with 1.0-2.0g of CuO (for oxidation) for at least 12hr in evacuated silica glass tubes.

The carbon isotopic compositions of the 101 micro-diamonds were

determined by MC-SIMS at the University of Edinburgh (EIMF) (71 diamonds) and the University of Alberta (CCIM) (42 diamonds) using Cameca 1270 and 1280 ion probes, respectively. Diamonds were mounted by pressing into indium, exposing polished surfaces or naturally flat diamond faces for analysis. The sample mounts were coated with a thin gold film prior to analysis. Samples were bombarded with a primary cesium ion beam with an impact energy of 20keV. Secondary ions were collected in multi-collection mode using Faraday cups for 5s per count cycle, with 20 cycles per analytical spot. Synthetic diamond with known carbon isotopic composition ($\delta^{13}C$ = -23.92 at EIMF and -22.576 ± 0.017 at CCIM) was used as external standard. Internal analytical precision for $\delta^{13}C$ analyses with SIMS at the University of Edinburgh is about ± 0.4‰ (2 sigma) and about ± 0.2‰ (2 sigma) at the University of Alberta.

An external standard was analyzed at the Stable Isotope Laboratory at the University of Alberta, EIMF and the CCIM for carbon isotopic composition to determine consistency between the three laboratories. It is observed that, relative to CCIM, a 0.15‰ and 0.04‰ bias exists between the EIMF and conventional sealed tube combustion analytical data sets, respectively, which are considered insignificant for the purpose of modelling and interpretations.

## 2.3. Physical Characteristics

### 2.3.1 Diamond Colour

The 209 diamonds from Artemisia are all transparent and range in colour from colourless to brown (Table 2.1). The brown, pink-brown and yellow diamonds range from light to dark shades of color. The majority of the diamonds (45%) are colourless, followed by yellow (20%), brown (14%) and pink-brown (6%) (Figure 2.2a); 14% of the diamonds could not be reliably characterized for

colour due to a combination of weak colouration and very small size.

The macro-diamond population is predominantly colourless followed by brown (20%), yellow (18%) and pink-brown (12%) colourations (Figure 2.2b). Among micro-diamonds, 30% of the stones were too small for reliable colour classification; otherwise, colourless diamonds dominate (40%), followed by yellow (22%) and brown (8%) (Figure 2.2c). The key difference between macro- and micro-diamonds is a strong apparent decrease in brown to pink-brown body colours and a less prominent decrease in colourless samples for diamonds ≤ 0.5mm. This apparent difference may be entirely due to difficulties in assessing body colour for very small samples (30% undetermined) and, therefore, is not evaluated further.

### 2.3.2 Diamond Morphology

Artemisia diamonds have octahedral (36%, Figure 2.3a), dodecahedral (19%, Figure 2.3d), twinned (macle, 13%, Figure 2.3b) and aggregated (intergrowth of two and more diamonds, 32%, Figure 2.3c) morphologies (Table 2.1; Figure 2.4a). Irregular (fragmented) diamonds were assigned to the above categories based on residual primary features.

Observed surface features include shield shaped laminae (stacked primary growth layers) on octahedral faces and plastic deformation lines on secondary dodecahedral surfaces (95%).

A comparison of macro- and micro-diamond morphologies (Figure 2.4b,c) shows that the relative proportion of macles and aggregates stays approximately constant, but that the proportion of dodecahedral (resorbed) diamonds decreases strongly from macro- (32%) to micro-diamonds (6%).

## 2.4. Carbon Isotopic Composition

Worldwide diamonds have a broad range in carbon isotopic composition from -41‰ (De Stefano et al., 2009) to +3‰ (Davies et al., 2003) with a distinct mode ~ -5‰ . Whilst eclogitic diamonds span this entire range (e.g., Cartigny, 2005), the carbon isotopic composition of peridotitic diamonds is more restricted, typically ranging from -10 to -2‰ (Kirkley et al., 1991; Cartigny et al., 1998 a,b).

The Artemisia diamond suite ranges in carbon isotopic composition from -24.5‰ to +1.6‰, with modes in classes (bins) -5.0 to -4.5‰ and -3.5 to -3.0‰, this bimodality is also reflected in cumulative probability curves (calculated using Isoplot version 2.2 by K.R. Ludwig) (Figure 2.5.). To reduce the effect of outliers, samples outside 2 sigma about the mean for both micro- and macro-diamonds were excluded and new averages calculated. A student t-test confirms that with 99% confidence the means of the two populations, -3.66‰ (micros) and -4.41‰ (macros), are not the same. Key differences between macro- and micro-diamonds are: (1.) although both modes are visible across the macro-/micro-diamond division, the main mode shifts from class -4.5 to -5.0‰ for macro-diamonds to class -3.0 to -3.5‰ for micro-diamonds, consistent with median values of -4.64‰ and -3.56‰ and skewness of -0.14 and 0.33, respectively (Figure 2.5). (2.) Macro-diamonds extend to strongly $^{13}C$ depleted compositions (range: -24.5 to -0.2‰) whilst micro-diamonds show a narrow compositional range extending to positive values (range -9.3 to 1.6‰, Figure 2.5).

## 2.5. Impurities

Nitrogen is the most common impurity in diamond. During diamond growth variable amounts of nitrogen may be incorporated into the crystal lattice as single substitutional impurities (Evans et al., 1981).Diamonds without

detectable nitrogen (<10ppm for micro-FTIR) are classified as Type II (Kaiser and Bond, 1959). At Artemisia, 44% of the diamonds are Type II (Table 2.1;Figure 2.6), with distinctly different abundances for macro- (21%) and micro-diamonds (68%). That these differences in nitrogen content are significant, and not just a result of small fluctuations in nitrogen concentration near the detection limit of FTIR, is implied by the observation of nitrogen contents >100 at. ppm in 43% of macro-diamonds and only 19% of micro-diamonds.

Diamonds with measureable nitrogen (Type I) are sub-divided based on their nitrogen aggregation state (Evans et al., 1981): diamonds containing predominantly singly substituted nitrogen (C-center) are classified as Type Ib and are extremely rare in nature. For diamonds containing aggregated nitrogen (Type Ia) there is a progression from pairs of nitrogen atoms (A-center, Type IaA) to rings of four nitrogen atoms about a vacancy (B-center, Type IaB) (Davies, 1976; Evans et al., 1981). Diamonds containing appreciable nitrogen in both the A- and B-centers (i.e., 10-90 %B) are classified as Type IaAB. The speed of the progression from nitrogen A- to B-centres is governed by a diamond's nitrogen content and the duration and time averaged temperature of its residence in the Earth's mantle (Evans and Harris, 1989). Therefore, from a genetic point of view, a binning of diamonds into the various sub-types (e.g. Type IaAB) without simultaneous evaluation of the absolute nitrogen content is meaningless and instead results are presented as a diagram of nitrogen content versus nitrogen aggregation state (Figure 2.7). Macro- and micro-diamonds from Artemisia show variable nitrogen contents (up to 1850 and 960 at. ppm, respectively) and both cover the full range in nitrogen aggregation from Type IaA to IaB.

Based on an assumed mantle residence time, nitrogen concentration-aggregation relationships may be employed to calculate time averaged residence

temperatures ($T_N$; Taylor et al, 1990; Leahy and Taylor 1997). Macro- and micro-diamonds (note that the majority of micro-diamonds are Type II for which $T_N$ cannot be derived) show a broad range in temperatures from about 1000 to 1450˚C around a common average of ~1218˚C (Figure 2.8). Using a 50˚C binning interval, the temperature distribution for micro-diamonds appears bimodal. A cumulative probability curve for micro-diamond $T_N$, however, does not indicate bimodality.

Platelets are defects in the diamond crystal lattice that form concurrently with the progression of nitrogen aggregation from A- to B-centers. Although their composition has been debated, platelet defects are now regarded as displaced interstitial carbon (Woods, 1986). Platelet defects (B' centers) are detected through a sharp absorbance peak between 1358 and 1380$cm^{-1}$. Type Ia Artemisia diamonds contain platelet defects in 31% of the total sample suite (Table 2.1), in both micro- (15%) and macro-diamonds (45%). For 'regular' diamonds, Woods (1986) recognized a linear relationship between the intensity of the platelet peak (I (B')) and the absorption coefficient at 1282 $cm^{-1}$ due to nitrogen present in B-centres. Samples falling below this line are considered as being "irregular" and having suffered "catastrophic platelet degradation" as a result of short lived heating events (Evans et al., 1995) or strain (Woods, 1986) at some point in their mantle residence history. Artemisia diamonds display characteristics of both 'normal' and 'irregular' diamonds. A linear correlation between platelet peak intensity and nitrogen present in B-center aggregation (expressed in at. ppm) is observed for most samples (Figure 2.9); some macro- and micro-diamonds, however, fall below this line indicating that an episode of platelet degradation had occurred at some point during their mantle residence history.

Hydrogen impurities in diamond are indicated by an infrared absorption

peak at 3107cm$^{-1}$, attributed to stretching vibrations of C=$CH_2$ bonds (Woods and Collins, 1983). For the diamonds from Artemisia, 67% of the samples contain hydrogen impurities (Table 2.1). The hydrogen peak at 3107cm$^{-1}$ is more abundant among macro-diamonds (94%) than among micro-diamonds (40%; Figure 2.10). Iakoubovskii and Adriaenssens (2002) observed a linear relationship between the intensity of the 3107cm$^{-1}$ hydrogen absorption peak and total nitrogen content for diamonds from the Argyle mine (Western Australia) and related this observation to an ammonium-rich growth environment. For Artemisia diamonds a similar correlation is not observed (Figure 2.10), with nitrogen-rich diamonds being commonly hydrogen poor.

## 2.6. Discussion

### 2.6.1 Carbon Isotopes

Carbon isotopic data are published for diamonds from the Lac de Gras kimberlite field in the Central Slave Province (Davies et al. 1999 and 2004; Donnelly et al., 2007; Cartigny et al. 2009), the Jericho kimberlite in the Northern Slave (De Stefano et al., 2009) and the Snap Lake kimberlite in the Southern Slave (Pokhilenko et al., 2004). In comparison, within a $\delta^{13}C$ range consistent with the majority of diamonds worldwide (-8‰ to +0‰) (Cartigny, 2005), the $\delta^{13}C$ distribution of Artemisia diamonds is shifted to $^{13}C$ enriched values relative to that observed from the Central Slave, though is consistent with the $\delta^{13}C$ distributions observed from the Southern and Northern Slave (Figure 2.11).

The variability of carbon isotopic distributions of diamonds from the Slave Craton may reflect tapping of carbon reservoirs with distinct isotopic compositions (e.g. mantle versus oceanic crust) and/or variation in the degree and style of isotopic fractionation prior to and during diamond precipitation. Both

open system isotopic fractionation of diamond forming fluid/melts (Galimov, 1991; Cartigny et al., 2001) and closed system fractionation during diamond precipitation (Deines, 1980; Thomassot et al., 2007; Stachel et al., 2009) have been invoked to explain observed carbon isotope frequency distributions.

Whilst on a worldwide scale, eclogitic and peridotitic diamonds have the same prominent mode in $\delta^{13}C$ at -5‰ (presumed to reflect the mantle value; e.g., Cartigny, 2005), eclogitic diamonds encompass a much broader range frequently extending to strongly $^{13}C$ depleted values (below -10‰, extending to -41‰); in contrast, only 1.3% of diamonds with peridotitic inclusions analysed from worldwide sources have $\delta^{13}C$ values below -10‰ (Stachel et al., 2009). At Artemisia, the occurrence of five macro-diamonds with $\delta^{13}C$ values in the range -14.2 to -24.5‰, therefore, strongly suggests the presence of an eclogitic component. Similar $^{13}C$ depleted values are not observed in the micro-diamond population.

Two main models have been proposed regarding the origin of isotopically light diamonds: (1.) the broad range in $\delta^{13}C$ exhibited by eclogitic diamonds suggests that subducted oceanic crust was a key source of diamond carbon. Organic and carbonaceous material may have been directly converted to eclogitic diamond during prograde metamorphism (e.g. Kirkley et al., 1991; McCandless and Gurney, 1997), with strongly $^{13}C$ depleted diamond representing the signature of former organic matter. As a variant of the subduction model, carbonates and graphitized former organic matter may have been mobilized during slab dehydration and/or melting and subsequently re-precipitated during redox reactions (c.f. Kesson and Ringwood, 1989). (2.) Alternatively, the formation of eclogitic diamonds relates to open system fractionation occurring during the separation of an unbuffered $CO_2$ fluid from a melt, that as a consequence becomes

increasingly depleted in $^{13}C$ (Javoy et al. 1986; Cartigny et al., 1998a). This model equally explains the almost exclusive restriction of highly negative $\delta^{13}C$ values to eclogitic (and rare webstertitic) diamonds, as $CO_2$ is buffered in olivine bearing diamond source rocks (Wyllie and Huang, 1976; Luth, 2003), precluding such open system fractionation in peridotites.

Micro-diamonds from Artemisia extend to $\delta^{13}C$ >0‰ (four samples), values very rarely observed globally but characteristic for so-called Group B (high-Ca eclogitic) diamonds from Bingara and Wellington (SE Australia), which have been related to diamond formation in meta-rodingites during subduction (Davies et al., 2003).

The bulk of macro- and micro-diamonds at Artemisia falls into the range -5 to -3‰, carbon isotopic compositions common for both, peridotitic and eclogitic diamonds. The observed small shift towards values typically >-5‰ may be interpreted as an indication for the involvement of slab derived, carbonate bearing fluids/melts in diamond formation (e.g. Stachel et al. 2009), but is not indicative of source paragenesis.

### 2.6.2 Nitrogen Characteristics

Nitrogen thermometry requires an estimate of a diamond's mantle residence time as an input parameter. Neither the Artemisia kimberlite nor its diamonds have been dated; our choice of a mantle residence time, therefore, had to be based on indirect evidence. From the carbon isotopic data we can conclude that Artemisia diamonds are at least in part of eclogitic paragenesis. Helmstaedt and Gurney (1995) suggest that the Mackenzie large igneous province, a short-lived massive igneous event affecting the Northern Slave ~1270Ma (LeCheminant and Heaman, 1989), was likely mantle-root destructive. Assuming that Artemisia

has a similar Eocambrian emplacement age as the nearest dated kimberlite in the Coronation Gulf Field (Anuri, see above), we set the mantle residence for Artemisia diamonds to ~500Ma, i.e. diamond formation subsequent to the Mackenzie event. This estimate obviously carries a large uncertainty, but the choice of a particular residence time actually has only a small influence on $T_N$; increasing the mantle residence time, e.g.from 0.5 to 1Ga decreases calculated temperatures on average by only 20˚C.

Nitrogen thermometry shows that Type Ia micro- and macro-diamonds from Artemisia reflect a wide range in mantle residence temperatures suggestive of sampling over a large depth interval (Figure 2.7 and 2.8). The micro- and macro-diamonds share similar average residence temperatures of ~1218 ±74°C and very similar peaks in their cumulative probability curves (Figure 2.8). A student t-test indicates that with 99% confidence the mean average residence temperatures of the micro- and macro-diamonds from Artemisia are the same. These results are slightly higher but within error of nitrogen and silicate inclusion based thermometric estimates for eclogitic and peridotitic diamonds from worldwide sources (Stachel and Harris, 2008).

A significant proportion (44%) of Artemisia diamonds are Type II (nitrogen ≤10 at. ppm). Type II diamonds comprise 2% of diamonds worldwide (Wilks and Wilks, 1991) Among inclusion bearing diamonds studied with micro-FTIR, this percentage is much higher, with 10% of eclogitic and 24% of peridotitic diamonds classifying as Type II (Stachel and Harris, 2009). Type II diamonds have been associated with a deep (sublithospheric) origin at a number of localities (e.g. Davies et al., 1999; Hutchison et al., 1999; Stachel et al., 2002; Banas et al., 2007), based on the observation of inclusions of majoritic garnet (deep asthenosphere and transition zone) and the assemblage ferropericlase,

CaSi-perovskite and MgSi-perovskite (lower mantle). In the absence of mineral inclusions, we cannot constrain if the high proportion of Type II diamonds at Artemisia relates to an unusual lithospheric growth environment, or if it reflects tapping of sublithospheric sources, which then would be particularly well represented among micro-diamonds.

### 2.6.3 The Micro-/Macro-Diamond Relationship

Our study of colouration for Artemisia macro-/micro-diamonds did not yield conclusive results, since an accurate and reproducible determination of light body colours is not possible for diamonds only a few hundred micrometers in size. A comparison of crystal forms between micro- and macro-diamonds shows a higher level of resorption (dodecahedral morphology) among macro-diamonds. The same relationship – micro-diamonds being less resorbed than macro-diamonds – has previously been observed in other deposits and was linked to a late stage release of micro-diamonds through disaggregation of mantle xenoliths, with early released micro-diamonds being completely destroyed through very rapid dissolution (Haggerty, 1986; McCandless et al., 1994). Otherwise, the morphological characteristics of micro- and macro-diamonds are not significantly different.

The carbon isotopic signature of micro- and macro-diamonds suggests some discrepancy in sources. The exclusive occurrence of isotopically light carbon in macro-diamonds and the restriction of positive $\delta^{13}C$ values to micro-diamonds clearly document that not all diamond sources are equally represented across the studied range of diamond sizes. Apart from a slight shift towards a second mode in class -3.5 to -3.0‰, which is dominant for micro-diamonds, the bulk of the micro- and macro-diamonds is indistinguishable in their $\delta^{13}C$

characteristics.

With respect to nitrogen contents, a clear difference exists between micro- and macro-diamonds. Micro-diamonds have a distinctly higher proportion of Type II diamonds and are overall lower in nitrogen than macro-diamonds. A high proportion of Type II micro-diamonds was previously observed by Trautman et al. (1997) for kimberlites (Aries, Emu 2) and lamproites (Argyle, Ellendale 4, Walgidee Hills) from north-western Australia, accounting for >45% and >95% of the respective micro-diamond suites.

The relative intensity of platelet related absorption in Type Ia diamonds implies that a sub-population of both micro- and macro-diamonds experienced platelet degradation, as a result of a short lived heating event and/or strain (Woods, 1986; Leahy and Taylor, 1997). As micro- and macro-diamonds show indistinguishable platelet characteristics and time averaged nitrogen residence temperatures, it is implied that Type Ia micro- and macro-diamonds had the same mantle residence history. Whether this conclusion extends to Type II diamonds cannot be assessed.

Employing the presence or absence of a hydrogen related absorption peak at 3107 $cm^{-1}$ as a finger print clearly separates macro- and micro-diamonds, with 94% of the former and only 40% of the latter containing detectable hydrogen.

The suggestion that micro-and macro-diamonds partially or wholly derive from different sources is not new and distinct mechanisms for the formation of micro-diamonds have been discussed in literature. Haggerty (1986) suggested that euhedral micro-diamonds precipitate during the reduction of C-bearing volatile rich fluids as they encounter the cooler and more reducing base of the lithosphere during upward percolation. This process was suggested to occur shortly prior to their entrainment as xenocrysts in kimberlitic magma and

consequently it was predicted that such micro-diamonds should be Type Ib (nitrogen not aggregated). Pattison and Levinson (1995) proposed that euhedral micro-diamonds form as phenocrysts in kimberlite, either directly from the melt or as condensates from fluids liberated from the carbon-bearing magma during decompression. The resorption of macro-diamonds was suggested as a possible carbon source for 'phenocrystic' micro-diamonds (Pattison and Levinson, 1995). Phenocrystic micro-diamonds by definition would be of the same age as the host kimberlite and, therefore, would have to be either Type Ib or Type II, and they would possibly have similar $\delta^{13}C$ compositions as their macro-diamond counterparts. This late stage phenocryst model implies an absence of resorption and etch features on micro-diamond surfaces. A commonly "euhedral" appearance of micro-diamonds can be readily explained without requiring a phenocrystic origin, if late stage release from mantle xenoliths/xenocrysts is considered (see above). As a variant of this model, the bulk of micro-diamonds in kimberlite samples may still reside in micro-xenoliths and xenocrysts and only become liberated during caustic fusion, acid digestion or fine crushing; protected by their host minerals/xenoliths, such micro-diamonds would have never been exposed to the transporting kimberlite magma.

The evidence that Type Ia macro- and micro-diamonds at Artemisia show similar and on average advanced nitrogen aggregation states is not consistent with micro-diamond precipitation just before or during kimberlite activity, but suggests that the two diamond size fractions formed broadly coeval. Yet, differences between micro- and macro-diamonds exist at Artemisia in the abundance of nitrogen and hydrogen free diamonds and in the extreme ends of $\delta^{13}C$ distributions. Different relative proportions of certain subpopulations (e.g., Type II diamonds) in dependence of diamond size and small subpopulations

unique to either micro- or macro-diamonds (e.g., diamonds with $\delta^{13}C$ >0 and <-10, respectively) are, therefore, indicated.

### 2.7. Conclusions

Micro- and macro-diamonds from the Artemisia kimberlite are overall similar with respect to nitrogen aggregation and modes in carbon isotopic composition, suggesting an overall common origin. Distinct geochemical signatures with respect to nitrogen content and strongly $^{13}C$ depleted and enriched compositions imply, however, that certain subpopulations are preferentially sampled or preserved in certain size fractions.

For the application of micro-diamond data in the evaluation of new kimberlite discoveries our study implies:

(1.) A low degree of resorption observed for micro-diamonds does not extend to macro-diamond size fractions and, therefore, very little information can be gleaned from micro-diamonds with respect to the quality of a deposits potential future diamond production.

(2.) Multiple diamond populations are mixed to form a deposits overall diamond content. The relative proportions of these different components vary with stone size and, based on the strong variation in the abundance of Type II and hydrogen bearing diamonds observed at Artemisia, there may be only limited communality between micro- and macro-diamonds. This implies that log-normal stone size frequency distributions, as observed for Artemisia, are not a reflection of a common origin of micro- and macro-diamonds.

## References

Araujo, D.P., Griffin, W.L., O'Reilly, S.Y., Grant, K.J., Ireland, T., Holden, P., van Acterbergh, E. 2009. Microinclusions in monocrystalline octahedral diamonds and coated diamonds from Diavik, Slave Craton: Clues to diamond genesis. Lithos 112(S2): 724-735

Banas, A., Stachel, T., Muehlenbachs, K., McCandless, T.E., 2007. Diamonds from the Buffalo Head Hills, Alberta: Formation in a non-conventional setting. Lithos, 93 (1-2):199-213

Bleeker, W., Hall, B. 2007. The Slave Craton; geology and metallogenic evolution, In Goodfellow, W.D. (ed.), Mineral Deposits of Canada: A Synthesis of Major Deposit-Types, District Metallogency, The Evolution of Geological Provinces and Exploration Methods: Geological Association of Canada, Mineral Deposits Division, Special Publication No. 5, pp.849-879

Boyd, S.R., Kiflawa, I., Woods, G.S. 1994. The relationship between infrared absorption and the A defect concentration in diamond. Philosophical Magazine Part B 69(6): 1149-1153

Boyd, S.R., Kiflawa, I., Woods, G.S. 1995. Infrared-absorption by the B-nitrogen aggregate in diamond. Philosophical Magazine Part B 72 (3): 351-361

Cartigny, P., 2005. Stable isotopes and the origin of diamonds. Elements 1(2):79-85

Cartigny, P., Harris, J.W., Javoy, M., 1998a. Eclogitic diamond formation at Jwaneng: no room for a recycled component. Science 280 (5368):1421-1424

Cartigny, P., Harries, J.W., Philips, D., Girard, M., Javoy, M. 1998b. Subduction related diamonds? The evidence from a mantle-derived origin from coupled $\delta^{13}C - \delta^{15}N$ determinations. Chemical Geology 147 (1-2):147-159

Cartigny, P., Harris, J.W., Javoy, M. 2001. Diamond genesis, mantle fractionations and mantle nitrogen content: A study of $\delta^{13}C$-N concentrations in diamonds. Earth and Planetary Science Letters 185: 85-98

Cartigny, P., Farquhar, J., Thomassot, E., Harris, J.W., Wing, B., Masterson, A. McKeegan, K., Stachel, T. 2009. The mantle origin for Paleoarchean peridotitic diamonds from the Panda kimberlite, Slave Craton: Evidence from $^{13}C$-, $^{15}N$- and $^{33,34}S$-stable isotope systematics. Lithos 112(S2): 852-864

Chapman, J.G., Boxer, G.L. 2004. Size distribution analyses for estimating diamond grade and value. Lithos 76: 368-375

Davies, G. 1976. The A nitrogen aggregate in diamond – its symmetry and possible structure. Journal of Physics Series C: Solid State Physics 9: L537-L542.

Davies, R.M., Griffin, W. l., Pearson, N.J., Andrew, A.S., Doyle, B.J., O'Reilly, S.Y. 1999. Diamonds from the deep pipe: pipe DO-27, Slave Craton, Canada, In: Gurney, J.J., Gurney, J.L., Pascoe, M.D., Richardson, S.H. (eds.), The J.B. Dawson Volume, Proceedings of the VIIth International Kimberlite Conference. Red Roof Design, Cape Town, pp. 148-155

Davies, R.M., Griffin, W.L., O'Reilly, S.Y., Andrew, A.S. 2003. Unusual mineral inclusions and carbon isotopes of alluvial diamonds from Bingara, eastern Australia. Lithos 69 (1-2): 51-66

Davies, R.M., Griffin, W.L., O'Reilly, S.Y., Doyle, B.J. 2004. Mineral inclusions and geochemical characteristics of micro-diamonds from the DO27, A154, A21, A418, DO18, DD17 and Ranch Lake kimberlites at Lac de Gras, Slave Craton, Canada. Lithos 77: 39-55

Deakin, A. S., G. L. Boxer 1989. Argyle AK1 diamond size distribution: the use of fine diamonds to predict the occurrence of commercial sized diamonds. In: Ross, J., Jaques, A.L., Ferguson, J., Green, D.H., O'Reilly, S.Y., Danchin, R.V., Janse, A.J.A. (eds.) Kimberlites and Related Rocks, Geological Society of Australia, Special Publication Vol.14, Blackwell Carlton (1989), pp.1117-1122

Deines, P. 1980. The carbon isotopic composition of diamonds: relationship to diamond shape, colour, occurrence and vapour composition. Geochimica et Cosmochimica Acta 44:943-961

De Stefano, A., Kopylova, M.G., Cartigny, P., Afanasiev, V. 2009. Diamonds and eclogites of the Jericho kimberlite (Northern Canada). Contributions to Mineralogy and Petrology 18: 295-315

Donnelly, C.L., Stachel, T., Creighton, S., Muehlenbachs, K., Whiteford, S. 2007. Diamonds and their mineral inclusions from the A154 South pipe, Diavik Diamond Mine, Northwest Territories, Canada. Lithos 98 (1):160:176

Evans, T. Qi, Z., Maguire, J. 1981. The stages of nitrogen aggregation in diamond. Journal of Physics Series C: Solid State Physics 14(12): L379-L384

Evans, T., Harris, J.W., 1989. Nitrogen aggregation, inclusion equilibration temperatures and the age of diamonds. In: Ross, J., Jaques, A.L., Ferguson, J., Green, D.H., O'Reilly, S.Y., Dachin, R.V., Janse, A.J.A.(eds.) Kimberlite and Related Rocks, Geological Society of Australia, Special Publication Vol. 14, Blackwell Carlton (1989), pp. 1001-1006

Evans, T., Kiflawi, I., Luyten, W., Vantendeloo, G., Woods, G.S., 1995. Conversion of platelets into dislocation loops and voidite formation in Type IaB diamonds. Proceedings of the Royal Society of London Series A 449: 295-313

Galimov, E.M. 1991. Isotope fractionation related to kimberlite magmatism and diamond formation. Geochimica et Cosmochimica Acta 55: 1697-1708

Grütter, H.S., Apter, D.B., Kong, J. 1999. Crust-mantle coupling: evidence from mantle-derived xenocrystic garnets. In: Gurney, J.J., Gurney, J.L., Pascoe, M.D., Richardson, S.H. (eds.), The J.B. Dawson Volume, Proceedings of the VIIth International Kimberlite Conference. Red Roof Design, Cape Town, pp.307-313

Haggerty, S.E. 1986. Diamond genesis in a multiply constrained model. Nature 320 (6):34-38

Helmstaedt, H.H., Gurney, J.J. 1995. Geotectonic controls of primary diamond deposits: implications for are selection. Journal of Geochemical Exploration 53: 124-144

Hildebrand, R.S., Hoffman, P.F., Bowring, S.A. 1987. Tectono-magmatic evolution of the 1.9Ga Great Bear Magmatic Zone, Wopmay Orogen, Northwestern Canada. Journal of Volcanology and Geothermal Research 32: 99-118

Hoffman, P.F. 1987. Early Proterozoic fore deeps, foredeep magmatism, and Superior-type iron formations of the Canadian Shield. In Kröner, A. (ed.), Proterozoic Lithospheric Evolution: American Geophysical Union Geodynamic Monograph 17, pp. 85-98

Hoffman, P.F. 1998. United Plates of America, the birth of a craton: Early Proterozoic assembly and growth of Laurentia. Annual Reviews of Earth and Planetary Science Letters 16: 543-603

Hutchinson, M.T., Cartigny, P., Harris, J.W., 1999. Carbon and nitrogen compositions and physical characteristics of transition zone and lower mantle diamonds from Sao Luiz, Brazil. In: Gurney, J.J., Gurney, J.L., Pascoe, M.D., Richardson, S.H. (eds.), The J.B. Dawson Volume, Proceedings of the VIIth International kimberlite conference. Red Roof Design, Cape Town, pp. 372-382

Iakoubovskii, K., Adriaenssens, G.J. 2002. Optical characterization of natural Argyle diamonds. Diamonds and Related Materials 11(1): 125-131

Javoy, M., Pineay, F., Delorme, H., 1986. Carbon and nitrogen isotopes in the mantle. Chemical Geology 57 (1-2): 41-62

Kaiser, W., Bond, W.L. 1959. Nitrogen, a major impurity in common Type I diamond. Physical Review 115(4):857-863

Kesson, S.E., Ringwood, A.E. 1989. Slab-mantle interactions 2. The formation of diamond. Chemical Geology 78: 97-118

Kirkley, M. B. G., J.J., Otter, M.L., Hill, S.J., Daniels, L.R. 1991. The application of C isotope measurements to the identification of sources of C in diamonds: a review. Applied Geochemistry 6: 477-494

LeCheminant, A.N., Heaman, L.M. 1989. Mackenzie igneous events, Canada: Middle Proterozoic hotspot magmatism associated with ocean opening. Earth and Planetary Science Letters 96: 38-48

Leahy, K., Taylor, W.R. 1997. The influence of the Glennie domain deep structure on the diamonds in Saskatchewan kimberlites. Russian Geology and Geophysics 38 (2): 481-491

Luth, R.W. 2003. Mantle volatiles – distribution and consequences. In: Carlson, R.W. (ed.), The Mantle and Core. Treatise on Geochemistry. Elsevier, Amsterdam, pp.319-361

Masun, K.M., Doyle, B.J., Ball, S., Walker, S. 1994. The geology and mineralogy of the Anuri kimberlite, Nunavut, Canada. Lithos 76 (1-4), 75-97

McCandless, T.E., Waldman, M.A., Gurney, J.J. 1994. Macrodiamonds and microdiamonds from Murfreesboro lamproites, Arkansas: morphology, mineral inclusions, and carbon isotope geochemistry. In: Meyer, H.O.A, Leonardos, O.H.(eds.) Proceedings of the Fifth International Kimberlite Conference Vol. 2. pp 78-97

McCandless, T.E., Gurney, J.J. 1997. Diamond eclogites: comparison with carbonaceous chondrites, carbonaceous shales, and microbial carbon enriched MORB. Russian Geology and Geophysics 38(2), 371-381

McNeill, J., Pearson, D.G., Klein-BenDavid, O., Nowell, G.M., Ottley, C.J., Chinn, I. 2009. Quantitative analysis of trace element concentrations in some gem-quality diamonds. Journal of Physics: Condensed Matter 21(36), 13pp

Pattison, D.R.M., Levinson, A.A. 1995. Are euhedral microdiamonds formed during ascent and decompression of kimberlite magma? Implications of use of micro-diamonds in diamond grade estimation. Applied Geochemistry 10: 725-738

Pokhilenko, N.P., Sobolev, N.V., Reutsky, V.N., Hall, A.E., Taylor, L.A. 2004. Crystalline inclusions and the c isotope ratios in diamonds from the Snap Lake/King Lake kimberlite dyke system: evidence of ultra deep and enriched lithospheric mantle. Lithos 77:57-67

Sobolev, V.S., Sobolev, N.V. 1980. New proof on very deep subsidence of eclogitized crustal rocks. Doklady Akademii Nauk SSSR 250: 683-685

Sobolev, N.V., Loginova, A.M., Zedgenizov, D.A., Seryotkin, Y.V., Yefimova, E.S., Floss, C., Taylor, L.A. 2004. Mineral inclusions in microdiamonds and macrodiamonds from kimberlites of Yakuta: a comparative study. Lithos 77 (1-4): 225-242

Stachel, T., Harris, J.W., 2008. The origin of cratonic diamonds - Constraints from mineral inclusions. Ore Geology Reviews 34: 5-32

Stachel, T., Harris, J.W. 2009. Formation of diamond in the Earth's mantle. Journal of Physics Condensed Matter 21 (36), 10pp

Stachel, T., Harris, J.W., Aulbach, S., Deines, P. 2002. Kankan diamonds (Guinea) III: $\delta^{13}C$ and nitrogen characteristics of deep diamonds. Contributions to Mineralogy and Petrology 142 (4): 465-475

Stachel, T., Harris, J.W., Muehlenbachs, K. 2009. Sources of carbon in inclusion bearing diamonds. Lithos 112 (S2): 625-637

Taylor, W.R., Jaques, A.L., Ridd, M. 1990. Nitrogen-defect aggregation characteristics of some Australasian diamonds: Time-temperature constraints on the source regions of pipe and alluvial diamonds. American Mineralogist 75: 1290-1310

Thomassot, E., Cartigny, P., Harris, J.W., Viljoen, K.S. 2007. Methane-related diamond crystallization in the Earth's mantle: Stable isotope evidences from the single diamond bearing xenolith. Earth and Planetary Science Letters 257: 361-371

Trautman, R.L., Griffin, B.J., Taylor, W.R., Apetsius, Z.V., Smith, C.B., Lee, D.C. 1997. A comparison of the micro-diamonds from kimberlite and lamproite of Yakutia and Australia. Russian Geology and Geophysics 38(2):341-355

Ward, J., Clements, B., 2002. Technical report and recommendations Northern Slave Properties, Nunavut, Ashton Mining of Canada Inc, 57pp.

Wilks, E., Wilks, J. 1991. Properties and Applications of Diamond. Butterworth-Heinemann Ltd., Oxford, UK, 525pp.

Woods, G.S. 1986. Platelets and the infrared-absorption of type-Ia diamonds. Proceedings of the Royal Society of London, Series A 407 (1832):219-238

Woods, G.S., Collins, A.T. 1983. Infrared-absorption spectra of hydrogen complexes in Type-I diamonds. Journal of Physics and Chemistry of Solids 44 (5): 471-475

Wyllie, P.J., Huang, W.L. 1976. Carbonation and melting reactions in the system $CaO-MgO-SiO_2-CO_2$ at mantle pressures with geophysical and petrological applications. Contributions to Mineralogy and Petrology 54:79-107

**Table 2.1.** Physical and chemical characteristics of Artemisia diamonds

| Sample | Weight (mg) | Sieve Class (+mm) | Crystal Form | Colour | P.D | $\delta^{13}C$ (‰) | $N_T$ (ppm) | $N_B$ (ppm) | %B | Type | $T_N$ (500Ma) (°C) | Hydrogen Peak Area ($cm^{-2}$) | Platelet Peak Area ($cm^{-2}$) |
|---|---|---|---|---|---|---|---|---|---|---|---|---|---|
| Art-2 | 1.1 | 0.600 | M | c | n | -5.99 | 305 | 275 | 90 | IaB | 1246 | 12.7 | 7.0 |
| Art-3 | 0.8 | 0.600 | O(frag) | c | n | -6.39 | 329 | 319 | 97 | IaB | 1281 | 22.1 | |
| Art-4 | 0.4 | 0.600 | O | c | n | -4.85 | 155 | 93 | 60 | IaAB | 1215 | 8.5 | 5.4 |
| Art-5 | 1.3 | 0.600 | M | c | n | -5.16 | 1849 | 782 | 42 | IaAB | 1133 | 4.0 | 227.1 |
| Art-6 | 0.8 | 0.600 | D | c | y | -5.44 | 1534 | 34 | 2 | IaA | 1055 | 1.4 | 465.4 |
| Art-8 | 1.0 | 0.600 | O(frag) | c | n | -6.72 | 220 | 220 | 100 | IaB | 1328 | 25.4 | 5.9 |
| Art-11 | 0.7 | 0.600 | M | lpb | y | -4.30 | 53 | 6 | 12 | IaAB | 1180 | 1.5 | |
| Art-13 | 0.4 | 0.450 | Agg | y | n | -2.40 | 0 | 0 | 0 | II | | | |
| Art-14 | 0.5 | 0.450 | Agg | ly | n | -4.00 | 114 | 103 | 90 | IaB | 1275 | 7.9 | |
| Art-15 | 0.6 | 0.450 | Agg | c | n | -3.28 | 0 | 0 | 0 | II | | | |
| Art-16 | 0.2 | 0.450 | O | c | n | -4.17 | 0 | 0 | 0 | II | | | |
| Art-21 | 0.2 | 0.300 | O | c | n | -4.84 | 658 | 161 | 24 | IaAB | 1138 | 2.2 | 45.8 |
| Art-22 | 0.2 | 0.300 | Agg | lb | y | -4.47 | 61 | 33 | 54 | IaAB | 1234 | 1.0 | 5.1 |

**Table 2.1. cont.**

| Sample | Weight (mg) | Sieve Class (+mm) | Crystal Form | Colour | P.D | $\delta^{13}C$ (‰) | $N_T$ (ppm) | $N_B$ (ppm) | %B | Type | $T_N$ (500Ma) (°C) | Hydrogen Peak Area ($cm^{-2}$) | Platelet Peak Area ($cm^{-2}$) |
|---|---|---|---|---|---|---|---|---|---|---|---|---|---|
| Art-23 | 0.2 | 0.300 | D(frag) | c | y | -2.60 | 0 | 0 | 0 | II | | | |
| Art-25 | 0.1 | 0.300 | Agg | c | n | -3.44 | 36 | 20 | 56 | IaAB | 1252 | 5.0 | |
| Art-26 | 0.2 | 0.300 | O | lb | y | -3.83 | 39 | 24 | 60 | IaAB | 1254 | 6.9 | 1.6 |
| Art-27 | 0.1 | 0.300 | O | c | n | -3.24 | 608 | 174 | 29 | IaAB | 1146 | 30.3 | 112.6 |
| Art-28 | 0.2 | 0.300 | O | c | n | -2.99 | 12 | 12 | 100 | IaB | 1426 | | |
| Art-29 | 0.2 | 0.300 | D(frag) | lb | y | -2.24 | 0 | 0 | 0 | II | | | |
| Art-30 | 0.1 | 0.300 | Agg | c | n | -4.59 | 80 | 63 | 79 | IaAB | 1260 | | |
| Art-34 | | 0.212 | O | c | n | -2.40 | 0 | 0 | 0 | II | | | |
| Art-35 | 0.1 | 0.300 | O | c | n | -4.96 | 0 | 0 | 0 | II | | 0.0 | |
| Art-36 | 0.1 | 0.300 | Agg | lb | y | -4.03 | 0 | 0 | 0 | II | | 1.2 | |
| Art-37 | 0.2 | 0.300 | M | c | n | -3.38 | 0 | 0 | 0 | II | | | |
| Art-40 | 0.0 | 0.212 | D | c | n | -3.77 | 112 | 0 | 0 | IaA | 1098 | | |
| Art-41 | 0.1 | 0.212 | O | c | n | 0.26 | 0 | 0 | 0 | II | | | |

**Table 2.1. cont.**

| Sample | Weight (mg) | Sieve Class (+mm) | Crystal Form | Colour | P.D | $\delta^{13}C$ (‰) | $N_T$ (ppm) | $N_B$ (ppm) | %B | Type | $T_N$ (500Ma) (°C) | Hydrogen Peak Area ($cm^{-2}$) | Platelet Peak Area ($cm^{-2}$) |
|---|---|---|---|---|---|---|---|---|---|---|---|---|---|
| Art-42 | 0.0 | 0.212 | O | c | n | -3.42 | 198 | 71 | 36 | IaAB | 1183 | 6.9 | 60.4 |
| Art-43 | 0.0 | 0.212 | D | c | y | -4.46 | 425 | 57 | 14 | IaAB | 1132 | | 47.1 |
| Art-47 | 0.0 | 0.212 | Agg | c | n | 0.00 | 214 | 133 | 62 | IaAB | 1209 | 19.6 | |
| Art-48 | 0.0 | 0.212 | Agg | c | n | -3.00 | 0 | 0 | 0 | II | | | |
| Art-49 | 0.0 | 0.212 | Agg | c | n | -3.38 | 180 | 103 | 57 | IaAB | 1208 | 16.7 | 23.5 |
| Art-50 | 0.0 | 0.212 | O | c | n | -4.44 | 0 | 0 | 0 | II | | | |
| Art-51 | 0.0 | 0.212 | O | lb | y | -5.08 | 470 | 50 | 11 | IaAB | 1123 | 3.9 | 34.0 |
| Art-52 | 0.0 | 0.212 | Agg | ly | n | -3.80 | 0 | 0 | 0 | II | | 3.6 | |
| Art-54 | 0.0 | 0.212 | M | c | n | -3.35 | 0 | 0 | 0 | II | | | |
| Art-55 | 0.1 | 0.212 | Agg | ly | y | -1.46 | 0 | 0 | 0 | II | | 5.7 | |
| Art-56 | 0.0 | 0.212 | O(frag) | c | n | -3.19 | 0 | 0 | 0 | II | | | |
| Art-58 | 0.1 | 0.212 | M | ly | n | -4.41 | 75 | 73 | 97 | IaB | 1327 | 0.9 | |
| Art-59 | 0.1 | 0.212 | Agg | ly | n | -4.36 | 0 | 0 | 0 | II | | | |

**Table 2.1. cont.**

| Sample | Weight (mg) | Sieve Class (+mm) | Crystal Form | Colour | P.D | $\delta^{13}C$ (‰) | $N_T$ (ppm) | $N_B$ (ppm) | %B | Type | $T_N$ (500Ma) (°C) | Hydrogen Peak Area ($cm^{-2}$) | Platelet Peak Area ($cm^{-2}$) |
|---|---|---|---|---|---|---|---|---|---|---|---|---|---|
| Art-60 | 0.1 | 0.212 | O | c | n | -1.21 | 0 | 0 | 0 | II | | 1.5 | |
| Art-62 | 0.0 | 0.212 | Agg | ly | n | 0.34 | 0 | 0 | 0 | II | | 0.8 | |
| Art-63 | 0.0 | 0.212 | O | c | n | -4.96 | 0 | 0 | 0 | II | | | |
| Art-64 | 0.0 | 0.212 | O(frag) | ly | n | -2.22 | 0 | 0 | 0 | II | | 3.2 | |
| Art-65 | 0.1 | 0.212 | Agg | ly | n | -2.58 | 0 | 0 | 0 | II | | | |
| Art-66 | 0.0 | 0.212 | O(frag) | c | n | -3.35 | 0 | 0 | 0 | II | | | |
| Art-67 | 0.1 | 0.212 | Agg | lb | y | -0.51 | 0 | 0 | 0 | II | | 0.9 | |
| Art-68 | 0.0 | 0.212 | D | ly | y | -4.17 | 181 | 100 | 55 | IaAB | 1206 | 2.7 | 40.7 |
| Art-69 | 0.0 | 0.212 | Agg | c | n | -2.71 | 0 | 0 | 0 | II | | 2.0 | |
| Art-70 | 0.1 | 0.212 | O | c | n | -2.39 | 645 | 62 | 10 | IaA | 1113 | 3.1 | 84.9 |
| Art-71 | 0.0 | 0.150 | Agg | c | n | -5.23 | 0 | 0 | 0 | II | | | |
| Art-72 | 0.0 | 0.150 | O(frag) | c | n | 0.20 | 0 | 0 | 0 | II | | | |
| Art-73 | 0.0 | 0.150 | O | ly | y | -3.15 | 0 | 0 | 0 | II | | | |

**Table 2.1. cont.**

| Sample | Weight (mg) | Sieve Class (+mm) | Crystal Form | Colour | P.D | $\delta^{13}C$ (‰) | $N_T$ (ppm) | $N_B$ (ppm) | %B | Type | $T_N$ (500Ma) (°C) | Hydrogen Peak Area ($cm^{-2}$) | Platelet Peak Area ($cm^{-2}$) |
|---|---|---|---|---|---|---|---|---|---|---|---|---|---|
| Art-74 | 0.0 | 0.150 | M(frag) | ly | n | -4.40 | 0 | 0 | 0 | II | | | |
| Art-75 | 0.0 | 0.150 | O | ly | n | -2.78 | 0 | 0 | 0 | II | | | |
| Art-76 | 0.2 | 0.150 | O(frag) | c | n | -2.32 | 678 | 257 | 38 | IaAB | 1152 | 0.1 | 105.6 |
| Art-77 | 0.0 | 0.150 | D | ly | n | -4.77 | 202 | 140 | 69 | IaAB | 1219 | 16.1 | |
| Art-80 | 0.0 | 0.150 | Agg | c | n | -9.32 | 0 | 0 | 0 | II | | | |
| Art-81 | 0.0 | 0.150 | M | ly | n | -5.30 | 0 | 0 | 0 | II | | | |
| Art-82 | 0.0 | 0.150 | O | c | n | -3.05 | 0 | 0 | 0 | II | | | |
| Art-83 | 0.0 | 0.150 | M | ly | n | -4.44 | 717 | 147 | 20 | IaAB | 1130 | | |
| Art-84 | 0.0 | 0.150 | O | c | n | -3.57 | 0 | 0 | 0 | II | | 6.1 | |
| Art-92 | 0.0 | 0.150 | O(frag) | c | n | -3.34 | 0 | 0 | 0 | II | | | |
| Art-94 | 0.0 | 0.150 | M | c | n | -6.50 | 212 | 181 | 85 | IaAB | 1244 | | |
| Art-95 | 0.0 | 0.150 | O | c | n | -4.70 | 175 | 138 | 79 | IaAB | 1237 | | |
| Art-96 | 0.0 | 0.150 | Agg | ly | n | -4.55 | 0 | 0 | 0 | II | | 36.0 | |

**Table 2.1. cont.**

| Sample | Weight (mg) | Sieve Class (+mm) | Crystal Form | Colour | P.D | $\delta^{13}C$ (‰) | $N_T$ (ppm) | $N_B$ (ppm) | %B | Type | $T_N$ (500Ma) (°C) | Hydrogen Peak Area ($cm^{-2}$) | Platelet Peak Area ($cm^{-2}$) |
|---|---|---|---|---|---|---|---|---|---|---|---|---|---|
| Art-98 | 0.0 | 0.150 | M | ly | n | -4.62 | 0 | 0 | 0 | II | | 4.6 | |
| Art-110 | 0.0 | 0.212 | O | ly | n | -3.86 | 115 | 113 | 99 | IaB | 1349 | | |
| Art-112 | 0.0 | 0.212 | O | ly | n | -4.00 | 0 | 0 | 0 | II | | | |
| Art-114 | 0.0 | 0.212 | Agg | c | n | -3.87 | 0 | 0 | 0 | II | | | |
| Art-120 | 0.0 | 0.212 | O | c | n | -4.59 | 0 | 0 | 0 | II | | | |
| Art-123 | 0.0 | 0.212 | O | c | n | -3.38 | 237 | 62 | 26 | IaAB | 1166 | 6.6 | 38.1 |
| Art-124 | 0.0 | 0.212 | Agg | lb | y | -3.87 | 0 | 0 | 0 | II | | | |
| Art-125 | 0.0 | 0.212 | M | ly | n | -3.56 | 0 | 0 | 0 | II | | | |
| Art-127 | 0.0 | 0.212 | O | c | n | -3.62 | 452 | 136 | 30 | IaAB | 1155 | 6.9 | 61.7 |
| Art-130 | 0.0 | 0.212 | O | ly | n | -3.55 | 0 | 0 | 0 | II | | 7.0 | |
| Art-136 | 0.1 | 0.212 | Agg | ly | n | -4.92 | 0 | 0 | 0 | II | | | |
| Art-138 | 0.9 | 0.600 | O | c | n | -7.11 | 304 | 303 | 100 | IaB | 1318 | 14.8 | 3.2 |
| Art-139 | 0.8 | 0.600 | O | c | n | -4.64 | 294 | 140 | 48 | IaAB | 1185 | 7.2 | 76.8 |

**Table 2.1. cont.**

| Sample | Weight (mg) | Sieve Class (+mm) | Crystal Form | Colour | P.D | $\delta^{13}C$ (‰) | $N_T$ (ppm) | $N_B$ (ppm) | %B | Type | $T_N$ (500Ma) (°C) | Hydrogen Peak Area ($cm^{-2}$) | Platelet Peak Area ($cm^{-2}$) |
|---|---|---|---|---|---|---|---|---|---|---|---|---|---|
| Art-142 | 0.5 | 0.600 | O | lb | y | -2.06 | 300 | 181 | 61 | IaAB | 1199 | 4.4 | |
| Art-143 | 1.8 | 0.600 | D | c | y | -5.04 | 766 | 425 | 56 | IaAB | 1169 | 1.5 | 291.8 |
| Art-144 | 0.9 | 0.600 | O | ly | n | -24.50 | 41 | 37 | 89 | IaAB | 1302 | 6.2 | 2.3 |
| Art-146 | 0.7 | 0.600 | D | lb | y | -0.16 | 0 | 0 | 0 | II | | 3.3 | |
| Art-147 | 1.0 | 0.600 | Agg | ly | n | -4.46 | 23 | 21 | 90 | IaAB | 1324 | 3.0 | 0.6 |
| Art-148 | 0.9 | 0.600 | M | c | y | -3.86 | 0 | 0 | 0 | II | | 0.5 | |
| Art-149 | 0.8 | 0.600 | O | lb | y | -2.46 | 0 | 0 | 0 | II | | 1.8 | |
| Art-150 | 1.1 | 0.600 | D(frag) | y | n | -6.39 | 1505 | 213 | 14 | IaAB | 1102 | 34.9 | |
| Art-151 | 1.0 | 0.600 | Agg(frag) | lpb | y | -6.38 | 68 | 41 | 61 | IaAB | 1239 | 1.7 | 2.0 |
| Art-153 | 1.9 | 0.600 | D | c | y | -4.77 | 1110 | 44 | 4 | IaA | 1078 | 3.7 | 18.2 |
| Art-155 | 2.0 | 0.600 | O(frag) | c | n | -4.67 | 210 | 49 | 23 | IaAB | 1165 | 7.4 | 24.5 |
| Art-156 | 0.6 | 0.600 | O | c | n | -4.09 | 0 | 0 | 0 | II | | 0.6 | |
| Art-158 | 1.0 | 0.600 | Agg | c | n | -1.88 | 0 | 0 | 0 | II | | | |

**Table 2.1. cont.**

| Sample | Weight (mg) | Sieve Class (+mm) | Crystal Form | Colour | P.D | $\delta^{13}C$ (‰) | $N_T$ (ppm) | $N_B$ (ppm) | %B | Type | $T_N$ (500Ma) (°C) | Hydrogen Peak Area ($cm^{-2}$) | Platelet Peak Area ($cm^{-2}$) |
|---|---|---|---|---|---|---|---|---|---|---|---|---|---|
| Art-159 | 2.0 | 0.600 | D | c | y | -5.70 | 70 | 65 | 92 | IaB | 1295 | 8.9 | 1.6 |
| Art-160 | 1.5 | 0.600 | D | c | y | -6.01 | 0 | 0 | 0 | II | | 3.9 | |
| Art-162 | 0.5 | 0.600 | Agg | c | n | -1.23 | 0 | 0 | 0 | II | | 0.8 | |
| Art-164 | 0.9 | 0.600 | M | c | n | -14.23 | 530 | 254 | 48 | IaAB | 1170 | 20.2 | 150.2 |
| Art-165 | 0.8 | 0.600 | M | c | n | -3.52 | 37 | 37 | 100 | IaB | 1386 | 5.4 | 1.4 |
| Art-166 | 0.5 | 0.600 | M | lpb | y | -5.20 | 76 | 37 | 48 | IaAB | 1222 | 1.8 | 1.4 |
| Art-167 | 1.1 | 0.600 | D(frag) | ly | y | -5.35 | 37 | 26 | 70 | IaAB | 1268 | 8.6 | 7.1 |
| Art-168 | 0.8 | 0.600 | M | c | n | -5.17 | 31 | 27 | 87 | IaAB | 1305 | 5.0 | 1.8 |
| Art-169 | 0.7 | 0.600 | Agg | ly | y | -4.98 | 1140 | 873 | 77 | IaAB | 1183 | 7.2 | 441.6 |
| Art-170 | 0.7 | 0.600 | Agg | c | y | -3.40 | 0 | 0 | 0 | II | | 0.4 | |
| Art-171 | 0.8 | 0.600 | O | lpb | y | -3.23 | 47 | 42 | 88 | IaAB | 1295 | 7.6 | 1.5 |
| Art-172 | 0.8 | 0.600 | O | ly | n | -3.70 | 0 | 0 | 0 | II | | 1.5 | |
| Art-173 | 0.8 | 0.600 | O | c | n | -3.31 | 13 | 11 | 88 | IaAB | 133 | 5.4 | |

**Table 2.1. cont.**

| Sample | Weight (mg) | Sieve Class (+mm) | Crystal Form | Colour | P.D | $\delta^{13}C$ (‰) | $N_T$ (ppm) | $N_B$ (ppm) | %B | Type | $T_N$ (500Ma) (°C) | Hydrogen Peak Area ($cm^{-2}$) | Platelet Peak Area ($cm^{-2}$) |
|---|---|---|---|---|---|---|---|---|---|---|---|---|---|
| Art-174 | 0.6 | 0.600 | M | ly | n | -3.88 | 30 | 19 | 62 | IaAB | 1264 | 2.1 | |
| Art-175 | 1.3 | 0.600 | Agg | c | n | -4.73 | 129 | 49 | 38 | IaAB | 1196 | 15.2 | 3.7 |
| Art-176 | 0.9 | 0.600 | Agg | c | n | -21.31 | 55 | 34 | 61 | IaAB | 1245 | 7.1 | 15.6 |
| Art-177 | 0.8 | 0.600 | Agg | lb | y | -4.18 | 65 | 53 | 81 | IaAB | 1269 | 12.4 | 13.9 |
| Art-178 | 0.9 | 0.600 | Agg | c | n | -5.45 | 17 | 13 | 74 | IaAB | 1297 | 2.7 | |
| Art-179 | 0.7 | 0.600 | Agg | c | n | -3.69 | 0 | 0 | 0 | II | | 0.4 | |
| Art-180 | 0.8 | 0.600 | O | c | n | -4.95 | 22 | 20 | 95 | IaB | 1349 | 5.1 | |
| Art-182 | 3.1 | 0.850 | O | c | n | -5.07 | 217 | 72 | 33 | IaAB | 1177 | 4.8 | 51.9 |
| Art-183 | 1.6 | 1.180 | O | lb | y | -2.45 | 0 | 0 | 0 | II | | 4.1 | |
| Art-184 | 1.0 | 0.850 | M | c | n | -4.64 | 628 | 155 | 25 | IaAB | 1140 | 6.0 | 84.8 |
| Art-186 | 2.8 | 0.850 | O(frag) | c | y | -3.89 | 73 | 54 | 74 | IaAB | 1254 | 6.3 | |
| Art-188 | 1.3 | 0.850 | Agg | c | n | -2.82 | 84 | 69 | 82 | IaAB | 1264 | 4.7 | 5.0 |
| Art-189 | 2.6 | 0.850 | Agg(frag) | lb | y | -1.94 | 58 | 58 | 100 | IaB | 1371 | 5.6 | |

**Table 2.1. cont.**

| Sample | Weight (mg) | Sieve Class (+mm) | Crystal Form | Colour | P.D | $\delta^{13}C$ (‰) | $N_T$ (ppm) | $N_B$ (ppm) | %B | Type | $T_N$ (500Ma) (°C) | Hydrogen Peak Area ($cm^{-2}$) | Platelet Peak Area ($cm^{-2}$) |
|---|---|---|---|---|---|---|---|---|---|---|---|---|---|
| Art-190 | 1.9 | 0.850 | O(frag) | ly | n | -1.76 | 114 | 103 | 90 | IaB | 1275 | 6.9 | |
| Art-191 | 2.4 | 0.850 | Agg | c | n | -4.69 | 0 | 0 | 0 | II | | 2.4 | |
| Art-192 | 1.3 | 0.850 | O | ly | n | -4.23 | 42 | 8 | 19 | IaAB | 1200 | 1.6 | 2.0 |
| Art-193 | 1.8 | 0.850 | Agg | lb | y | -2.45 | 33 | 51 | 66 | IaAB | 1266 | 6.2 | |
| Art-194 | 2.5 | 0.850 | O(frag) | ly | n | -3.08 | 37 | 21 | 56 | IaAB | 1251 | 4.8 | 86.0 |
| Art-195 | 1.3 | 0.850 | Agg | lb | y | -6.77 | 81 | 81 | 100 | IaB | 1360 | 10.6 | |
| Art-196 | 4.5 | 1.180 | D | ly | y | -5.20 | 542 | 300 | 45 | IaAB | 1166 | 14.5 | 88.1 |
| Art-197 | 5.8 | 1.180 | Agg | c | n | -3.53 | 26 | 17 | 65 | IaAB | 1272 | 7.7 | |
| Art-198 | 1.7 | 0.850 | D | lb | y | -3.43 | 27 | 7 | 27 | IaAB | 1225 | 7.5 | |
| Art-199 | 2.7 | 0.850 | Agg | ly | n | -3.42 | 392 | 172 | 44 | IaAB | 1174 | | |
| Art-200 | 1.8 | 0.850 | Agg | c | n | -4.86 | 18 | 12 | 40 | IaAB | 1253 | 6.3 | |
| Art-201 | 1.8 | 0.850 | Agg | ly | n | -3.19 | 0 | 0 | 0 | II | | 0.6 | |
| Art-202 | 2.5 | 0.850 | D(frag) | lb | y | -4.49 | 1083 | 0 | 0 | IaA | 1047 | 10.4 | |

**Table 2.1. cont.**

| Sample | Weight (mg) | Sieve Class (+mm) | Crystal Form | Colour | P.D | $\delta^{13}C$ (‰) | $N_T$ (ppm) | $N_B$ (ppm) | %B | Type | $T_N$ (500Ma) (°C) | Hydrogen Peak Area ($cm^{-2}$) | Platelet Peak Area ($cm^{-2}$) |
|---|---|---|---|---|---|---|---|---|---|---|---|---|---|
| Art-203 | 1.9 | 0.850 | D(frag) | ly | y | -23.00 | 38 | 14 | 37 | IaAB | 1228 | 0.3 | |
| Art-204 | 2.6 | 0.850 | D(frag) | pb | y | -5.28 | 40 | 15 | 37 | IaAB | 1227 | 0.6 | |
| Art-205 | 1.1 | 0.850 | D(frag) | lb | y | -4.54 | 54 | 19 | 35 | IaAB | 1216 | 0.3 | |
| Art-206 | 1.3 | 0.850 | Agg | c | n | -4.66 | 0 | 0 | 0 | II | | | |
| Art-207 | 2.1 | 0.850 | D | lpb | y(2) | -4.33 | 888 | 207 | 23 | IaAB | 1129 | | 97.7 |
| Art-208 | 1.4 | 0.850 | D(frag) | dpb | y | -4.33 | 310 | 153 | 49 | IaAB | 1185 | 6.3 | 70.8 |
| Art-209 | 2.1 | 0.850 | Agg | c | n | -3.74 | 0 | 0 | 0 | II | | | |
| Art-210 | 2.4 | 0.850 | M | lb | y | -3.42 | 22 | 11 | 50 | IaAB | 1259 | 3.9 | |
| Art-211 | 5.0 | 0.850 | M | lb | y | -3.13 | 63 | 38 | 60 | IaAB | 1240 | 2.4 | |
| Art-212 | 1.4 | 0.850 | Agg | c | n | -5.17 | 0 | 0 | 0 | II | | 0.3 | |
| Art-214 | 4.2 | 0.850 | O(frag) | lb | y | -4.97 | 294 | 174 | 59 | IaAB | 1197 | 3.3 | 81.4 |
| Art-215 | 0.5 | 0.850 | Agg | c | n | -4.52 | 135 | 119 | 88 | IaAB | 1264 | 18.4 | |
| Art-216 | 3.9 | 0.850 | O(frag) | ly | n | -3.11 | 67 | 52 | 78 | IaAB | 1263 | 7.7 | |

**Table 2.1. cont.**

| Sample | Weight (mg) | Sieve Class (+mm) | Crystal Form | Colour | P.D | $\delta^{13}C$ (‰) | $N_T$ (ppm) | $N_B$ (ppm) | %B | Type | $T_N$ (500Ma) (°C) | Hydrogen Peak Area ($cm^{-2}$) | Platelet Peak Area ($cm^{-2}$) |
|---|---|---|---|---|---|---|---|---|---|---|---|---|---|
| Art-217 | 4.7 | 0.850 | D | dpb | y | -5.33 | 529 | 26 | 5 | IaA | 1100 | 1.2 | 30.2 |
| Art-218 | 3.1 | 0.850 | D | lpb | y | -1.92 | 0 | 0 | 0 | II | | 5.5 | |
| Art-220 | 2.1 | 0.850 | O(frag) | ly | n | -3.76 | 157 | 58 | 37 | IaAB | 1190 | 6.0 | 32.7 |
| Art-221 | 1.7 | 0.850 | D | c | y | -4.97 | 211 | 134 | 64 | IaAB | 1212 | 4.7 | 36.0 |
| Art-222 | 1.4 | 0.850 | D | c | y | -5.00 | 656 | 420 | 64 | IaAB | 1181 | 5.3 | 274.4 |
| Art-223 | 2.2 | 0.850 | O(frag) | c | n | -4.18 | 0 | 0 | 0 | II | | 1.2 | |
| Art-224 | 2.0 | 0.850 | Agg | ly | n | -5.25 | 228 | 40 | 18 | IaAB | 1155 | 24.0 | 15.7 |
| Art-225 | 3.1 | 0.850 | O | lb | y | -4.42 | 31 | 16 | 50 | IaAB | 1249 | 3.9 | |
| Art-226 | 3.2 | 0.850 | D | c | y | -4.43 | 250 | 147 | 59 | IaAB | 1201 | 3.7 | 82.0 |
| Art-227 | 3.7 | 0.850 | Agg | c | n | -5.10 | 359 | 253 | 71 | IaAB | 1206 | 6.6 | 128.7 |
| Art-228 | 2.8 | 0.850 | Agg | c | n | -4.34 | 29 | 9 | 30 | IaAB | 1227 | 3.1 | |
| Art-229 | 1.4 | 0.850 | O | ly | n | -5.59 | 743 | 471 | 63 | IaAB | 1117 | 2.3 | 321.6 |
| Art-230 | 1.0 | 0.850 | M | c | n | -5.70 | 95 | 24 | 25 | IaAB | 1188 | 1.1 | 4.3 |

**Table 2.1. cont.**

| Sample | Weight (mg) | Sieve Class (+mm) | Crystal Form | Colour | P.D | $\delta^{13}C$ (‰) | $N_T$ (ppm) | $N_B$ (ppm) | %B | Type | $T_N$ (500Ma) (°C) | Hydrogen Peak Area ($cm^{-2}$) | Platelet Peak Area ($cm^{-2}$) |
|---|---|---|---|---|---|---|---|---|---|---|---|---|---|
| Art-231 | 10.8 | 1.180 | D | dpb | y | -2.83 | 0 | 0 | 0 | II | | 4.4 | |
| Art-232 | 9.1 | 1.180 | Agg | lb | y | -4.97 | 0 | 0 | 0 | II | | 4.1 | |
| Art-233 | 2.9 | 1.180 | Agg | c | y | -8.29 | 0 | 0 | 0 | II | | 1.2 | |
| Art-234 | 6.6 | 1.180 | D | lb | y | -2.06 | 118 | 73 | 62 | IaAB | 1225 | 5.7 | 9.3 |
| Art-235 | 6.9 | 1.180 | D(frag) | lpb | y | -23.30 | 559 | 260 | 47 | IaAB | 1168 | 7.1 | 115.6 |
| Art-236 | 2.0 | 1.180 | Agg | c | n | -4.19 | 317 | 2 | 0 | IaA | 1074 | 0.3 | |
| Art-237 | 22.1 | 1.180 | D | ly | y | -3.45 | 980 | 510 | 52 | IaAB | 1158 | 2.3 | 297.5 |
| Art-238 | 3.0 | 1.180 | D | lpb | y | -6.22 | 790 | 46 | 6 | IaA | 1095 | 3.0 | 23.2 |
| Art-239 | 5.4 | 1.180 | D | b | y | -4.53 | 18 | 14 | 78 | IaAB | 1302 | 1.4 | |
| Art-240 | 4.1 | 1.180 | D | lb | y | -4.42 | 0 | 0 | 0 | II | | 4.7 | |
| Art-241 | 3.1 | 1.180 | Agg | c | n | -9.88 | 0 | 0 | 0 | II | | | |
| Art-242 | 3.3 | 1.180 | D | c | y | -4.74 | 346 | 202 | 58 | IaAB | 1192 | 6.0 | 87.2 |
| Art-243 | 15.1 | 1.700 | D | lpb | y | -4.64 | 705 | 168 | 24 | IaAB | 1136 | 72.7 | 31.4 |

**Table 2.1. cont.**

| Sample | Weight (mg) | Sieve Class (+mm) | Crystal Form | Colour | P.D | $\delta^{13}C$ (‰) | $N_T$ (ppm) | $N_B$ (ppm) | %B | Type | $T_N$ (500Ma) (°C) | Hydrogen Peak Area ($cm^{-2}$) | Platelet Peak Area ($cm^{-2}$) |
|---|---|---|---|---|---|---|---|---|---|---|---|---|---|
| Art-244 | 15.9 | 1.700 | D | c | y | -6.18 | 607 | 300 | 49 | IaAB | 1168 | 3.5 | 185.9 |
| Art-245 | 6.8 | 1.700 | D | vlb | n | -5.14 | 529 | 203 | 38 | IaAB | 1160 | 3.8 | 131.7 |
| Art-246 | 0.3 | 0.300 | O | lb | y | -2.61 | 0 | 0 | 0 | II | | 2.8 | |
| Art-247 | 0.1 | 0.300 | Agg | ly | n | -3.42 | 0 | 0 | 0 | II | | | |
| Art-248 | 0.7 | 0.600 | O | c | n | -4.94 | 67 | 62 | 92 | IaB | 1298 | 6.9 | |
| Art-249 | 0.9 | 0.600 | D | lb | y | -5.13 | 453 | 325 | 72 | IaAB | 1201 | 13.3 | 115.6 |
| Art-252 | 1.9 | 0.850 | O(frag) | c | n | -1.18 | 627 | 50 | 8 | IaA | 1108 | 2.1 | 39.7 |
| Art-253 | 1.1 | 0.850 | Agg | c | n | -3.39 | 74 | 72 | 97 | IaB | 1327 | 0.3 | |
| Art-255 | 3.1 | 1.180 | D | lb | y | -4.89 | 764 | 62 | 8 | IaA | 1103 | 1.0 | 16.4 |
| Art-256 | | 1.700 | O | c | n | -5.53 | 57 | 36 | 63 | IaAB | 1247 | | |
| ArtA | nd | 0.212 | Agg | nd | nd | 1.63 | 0 | 0 | 0 | II | | | |
| ArtAA | nd | 0.150 | M | nd | nd | -3.34 | 0 | 0 | 0 | II | | | |
| ArtAB | nd | 0.106 | Agg | nd | nd | -5.32 | 170 | 170 | 100 | IaB | 1336 | | |

**Table 2.1. cont.**

| Sample | Weight (mg) | Sieve Class (+mm) | Crystal Form | Colour | P.D | $\delta^{13}C$ (‰) | $N_T$ (ppm) | $N_B$ (ppm) | %B | Type | $T_N$ (500Ma) (°C) | Hydrogen Peak Area ($cm^{-2}$) | Platelet Peak Area ($cm^{-2}$) |
|---|---|---|---|---|---|---|---|---|---|---|---|---|---|
| ArtAC | nd | 0.150 | O | nd | nd | -2.69 | 0 | 0 | 0 | II | | | |
| ArtAD | nd | 0.106 | Agg | nd | nd | -2.62 | 0 | 0 | 0 | nd | | | |
| ArtAE | nd | 0.150 | O | nd | nd | -1.81 | 0 | 0 | 0 | II | | | |
| ArtB | nd | 0.212 | Agg | nd | nd | -4.49 | 0 | 0 | 0 | II | | | |
| ArtC | nd | 0.150 | O | nd | nd | -4.73 | 111 | 101 | 91 | IaB | 1279 | | |
| ArtD | nd | 0.212 | O | nd | nd | -4.21 | 0 | 0 | 0 | II | | | |
| ArtE | nd | 0.212 | O | nd | nd | -3.14 | 0 | 0 | 0 | II | | | |
| ArtF | nd | 0.106 | Agg | nd | nd | -4.71 | 0 | 0 | 0 | nd | | | |
| ArtG | nd | 0.106 | O | nd | nd | -3.77 | 0 | 0 | 0 | II | | | |
| ArtH | nd | 0.212 | O | nd | nd | -4.55 | 115 | 44 | 38 | IaAB | 1199 | 6.0 | 35.1 |
| ArtI | nd | 0.212 | M | nd | nd | -4.40 | 0 | 0 | 0 | II | | | |
| ArtJ | nd | 0.212 | M | nd | nd | -2.62 | 0 | 0 | 0 | II | | | |
| ArtK | nd | 0.212 | Agg | nd | nd | -3.44 | 0 | 0 | 0 | II | | | |

**Table 2.1. cont.**

| Sample | Weight (mg) | Sieve Class (+mm) | Crystal Form | Colour | P.D | $\delta^{13}C$ (‰) | $N_T$ (ppm) | $N_B$ (ppm) | %B | Type | $T_N$ (500Ma) (°C) | Hydrogen Peak Area ($cm^{-2}$) | Platelet Peak Area ($cm^{-2}$) |
|---|---|---|---|---|---|---|---|---|---|---|---|---|---|
| ArtL | nd | 0.150 | O | nd | nd | -3.85 | 0 | 0 | 0 | II | | | |
| ArtM/AF | nd | 0.212 | M | nd | nd | -2.43 | 0 | 0 | 0 | II | | | |
| ArtN | nd | 0.106 | O | nd | nd | -3.30 | 0 | 0 | 0 | II | | | |
| ArtO | nd | 0.106 | Agg | nd | nd | -3.33 | 0 | 0 | 0 | II | | | |
| ArtP | nd | 0.150 | O | nd | nd | -3.82 | 0 | 0 | 0 | II | | | |
| ArtQ | nd | 0.150 | O | nd | nd | -3.42 | 0 | 0 | 0 | II | | | |
| ArtR/S | nd | 0.150 | Agg | nd | nd | -3.21 | 959 | 606 | 63 | IaAB | 1170 | 18.5 | 62.0 |
| ArtT | nd | 0.212 | Agg | nd | nd | -4.59 | 0 | 0 | 0 | II | | | |
| ArtU | nd | 0.212 | Agg | nd | nd | -9.19 | 0 | 0 | 0 | II | | | |

**Table 2.1. cont.**

| Sample | Weight (mg) | Sieve Class (+mm) | Crystal Form | Colour | P.D | $\delta^{13}C$ (‰) | $N_T$ (ppm) | $N_B$ (ppm) | %B | Type | $T_N$ (500Ma) (°C) | Hydrogen Peak Area ($cm^{-2}$) | Platelet Peak Area ($cm^{-2}$) |
|---|---|---|---|---|---|---|---|---|---|---|---|---|---|
| ArtV | nd | 0.212 | O | nd | nd | -1.75 | 482 | 482 | 100 | IaB | 1304 | | |
| ArtW | nd | 0.212 | O | nd | nd | -4.72 | 0 | 0 | 0 | nd | | | |
| ArtX | nd | 0.106 | O | nd | nd | -4.57 | 848 | 295 | 35 | IaAB | 1145 | 2.1 | 60.2 |
| ArtY | nd | 0.150 | Agg | nd | nd | -4.58 | 0 | 0 | 0 | II | | | |
| ArtZ | nd | 0.212 | O | nd | nd | -3.18 | 0 | 0 | 0 | II | | | |

Agg = aggregate, (frag) = fragmented, O = octahedron, M = macle, D = dodecahedroid; c = colourless, vlb = very light brown, lb = light brown, b = brown, lpb = light pink-brown, pb = pink-brown, dpb = dark pink-brown, ly = light yellow, y = yellow; P.D. = plastic deformation, bd = below the limit of detection, nd = diamond too small to weigh/handle

## Figures

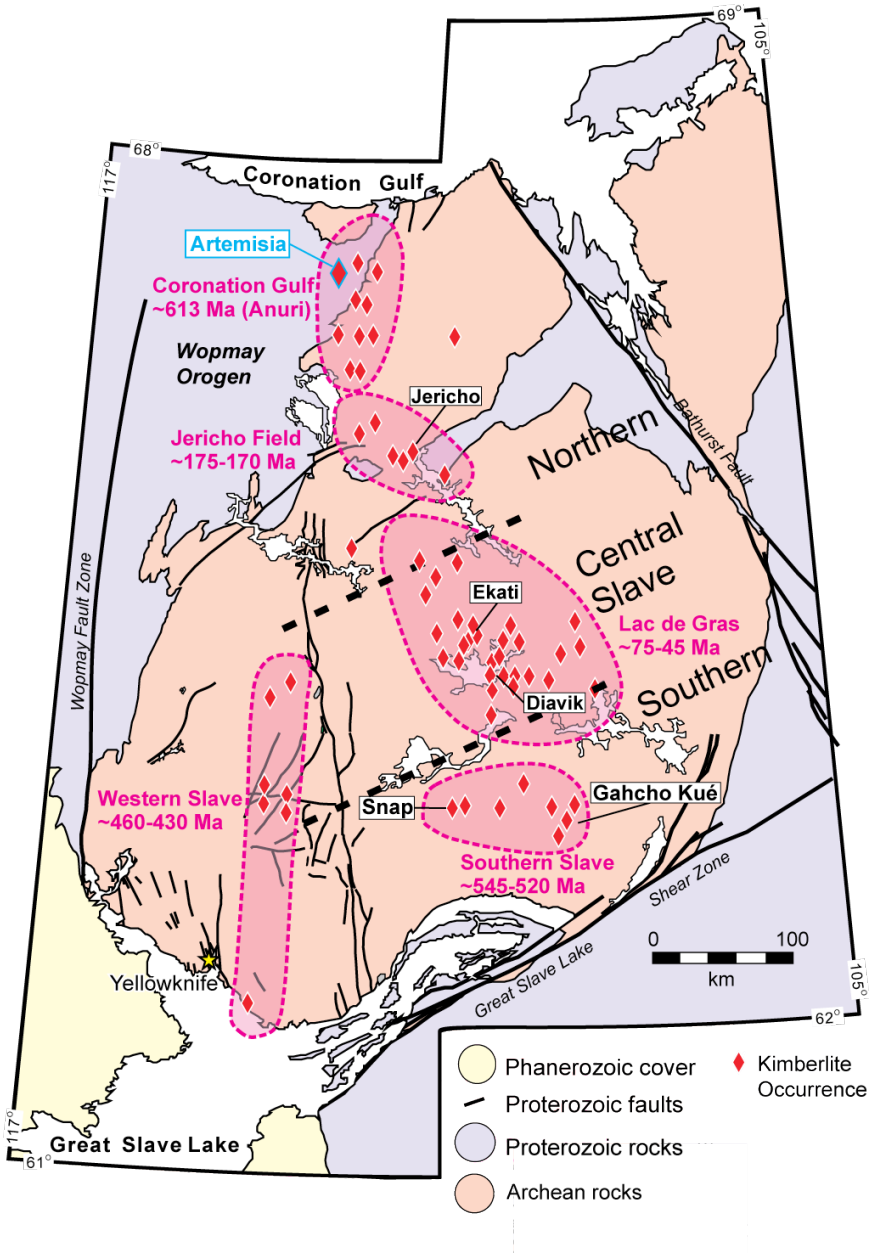


**Figure 2.1.** Map of kimberlite occurrences and kimberlite fields in the Slave Craton (modified after Bleeker and Hall, 2007). The location of Artemisia kimberlite within the Coronation Gulf Field is indicated

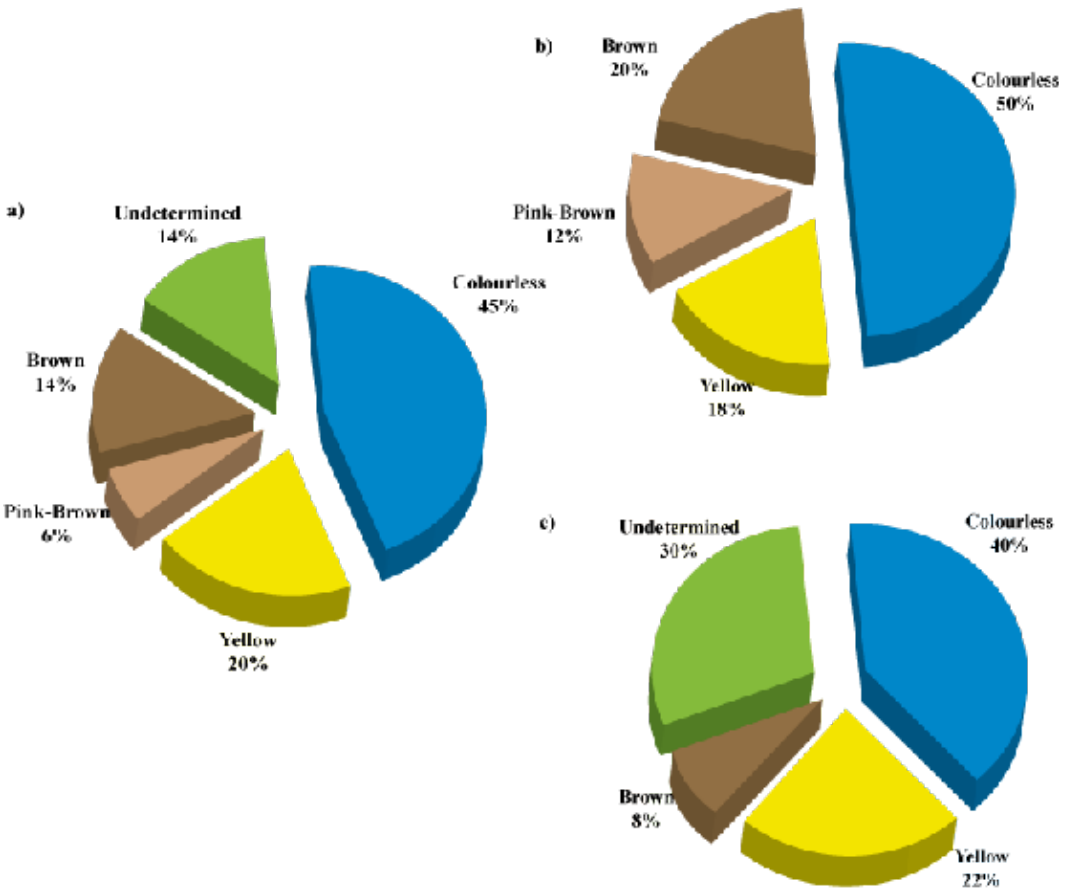


**Figure 2.2.** Colour of diamonds from Artemisia. a) All samples; b) Macro-diamonds; c) Micro-diamonds

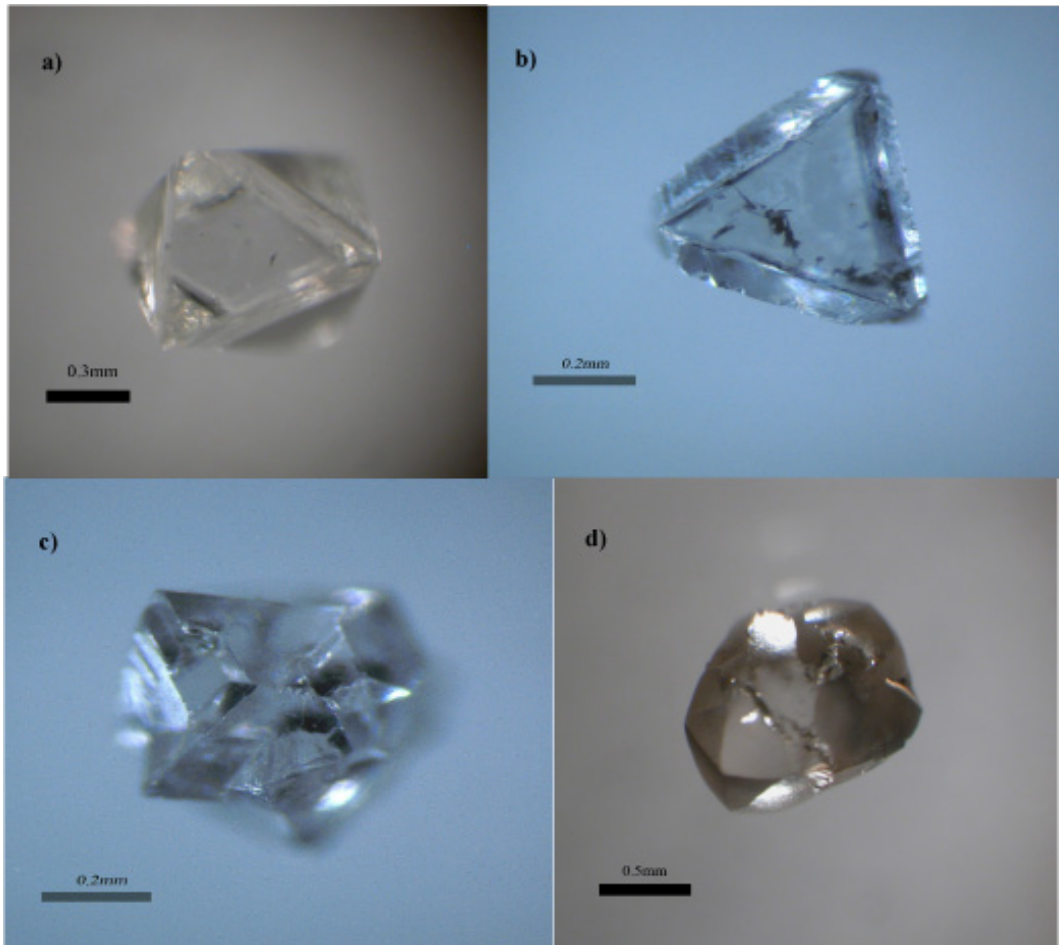


**Figure 2.3.** Examples of crystal forms observed for Artemisia diamonds. a) Octahedron (Art-138); b) Macle (Art-12); c) Aggregate (Art-13); d) Dodecahedroid (Art-234)

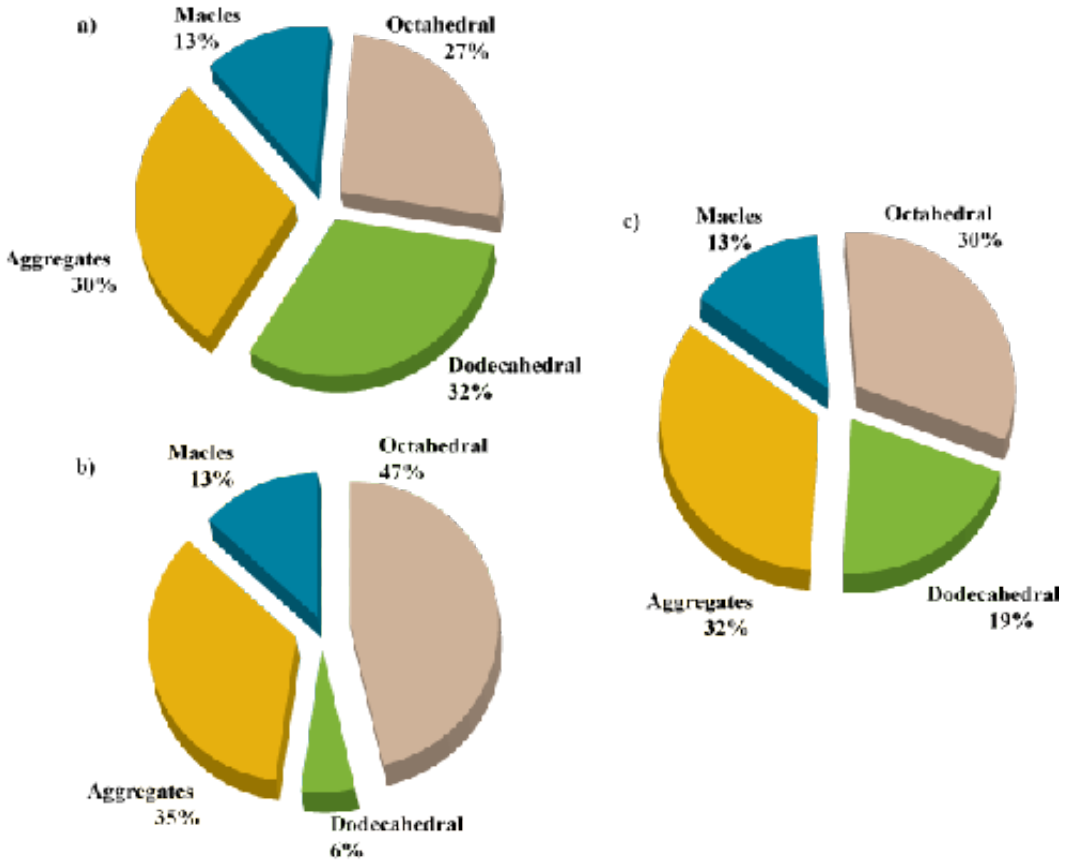


**Figure 2.4.** Morphology of Artemisia diamonds. a) Macro-diamonds (n=108); b) Micro-diamonds (n=101); c) All diamonds (n=209)

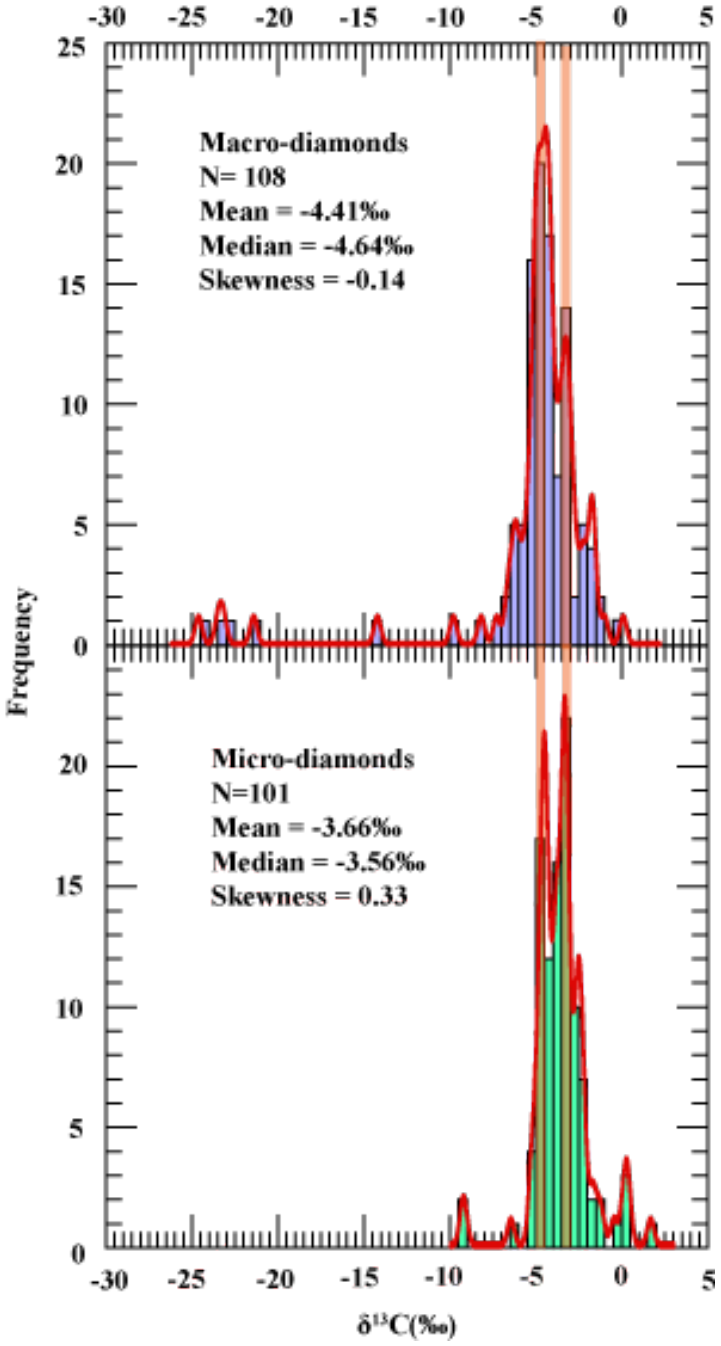


**Figure 2.5.** Histogram of carbon stable isotopic compositions of Artemisia diamonds. Two common modes are outlined in orange. Cumulative probability curves (red lines) were calculated using Isoplot version 2.2 by K.R. Ludwig.

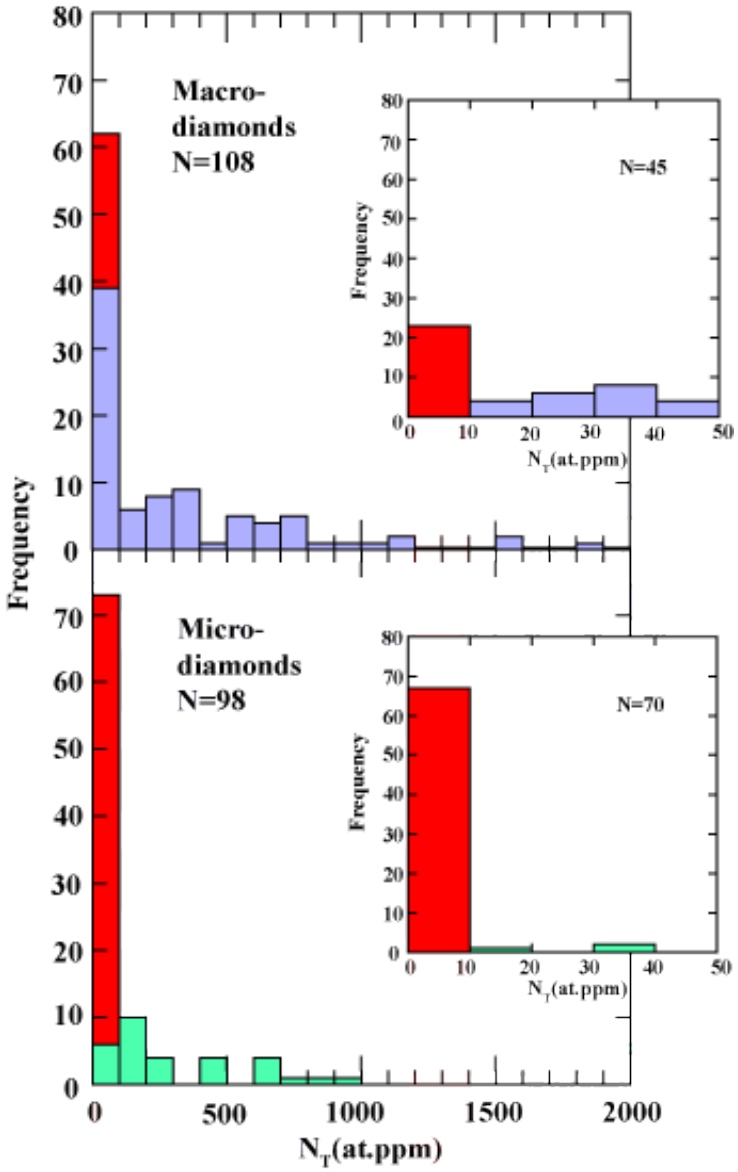


**Figure 2.6**. Total nitrogen content of micro-(bottom) and macro-diamonds (top) from Artemisia. Inset boxes: Total nitrogen content ranging from 0 to 50 at.ppm. Red denotes Type II diamonds.

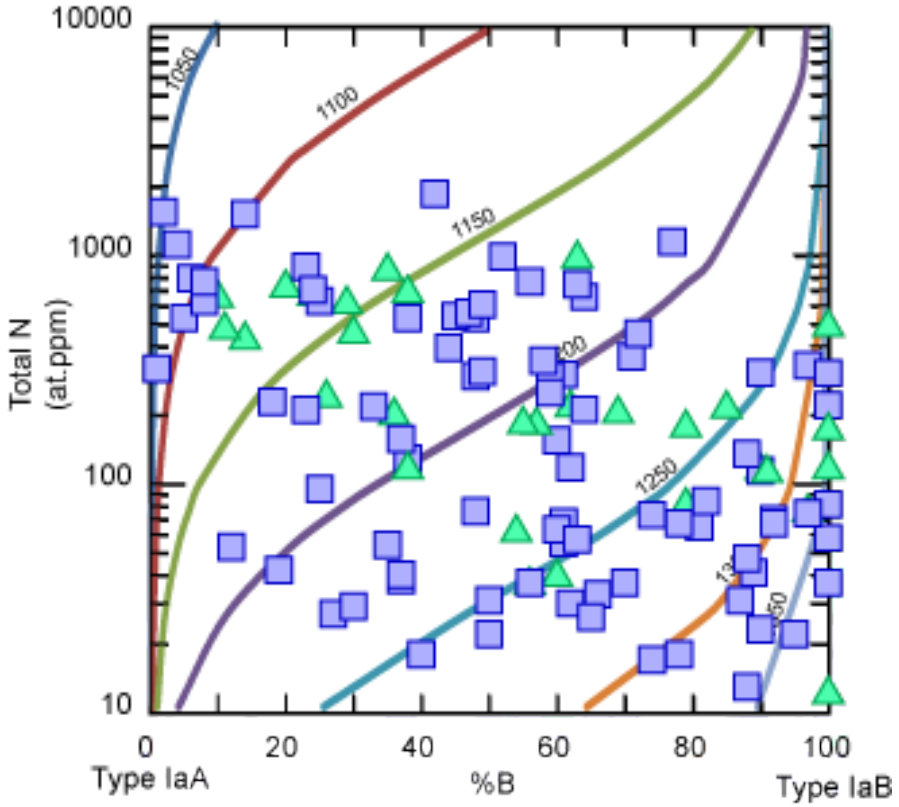


**Figure 2.7.** Total nitrogen content versus nitrogen aggregation state expressed as %B (the relative proportion of nitrogen in B centre: B/[A+B]). Isotherms based on 500 Ma mantle residence time are calculated after Leahy and Taylor (1997). Green triangle: micro-diamonds; Blue square: macro-diamond

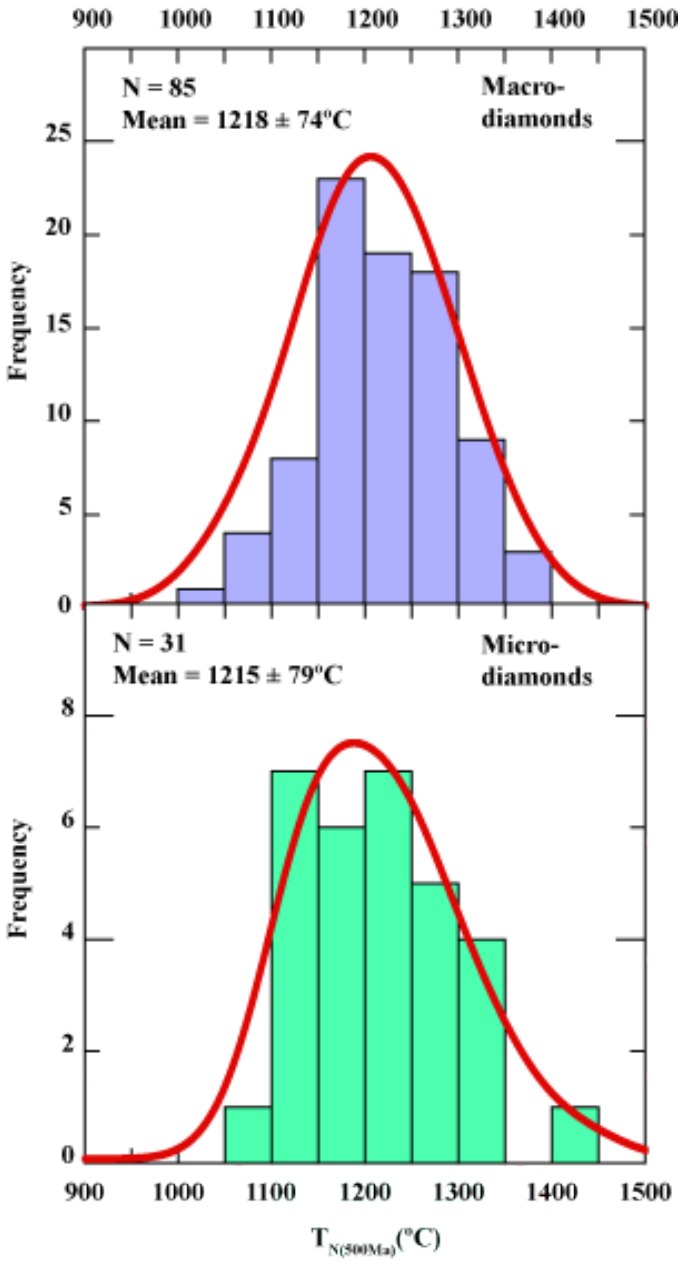


**Figure. 2.8.** Mantle residence temperatures ($T_N$) for Artemisia micro- and macro-diamonds calculated from nitrogen concentration-aggregation relationships (Leahy and Taylor, 1997) and assuming a mantle residence time of 500 Ma. Temperatures cannot be estimated for pure IaA (n=3) and IaB (n=8) diamonds and hence, for such samples aggregations was set to 1 and 99 %B respectively, yielding maximum (former) and minimum (latter) temperature estimates. Cumulative probability curves (red lines) were calculated using Isoplot version 2.2 by K.R. Ludwig.

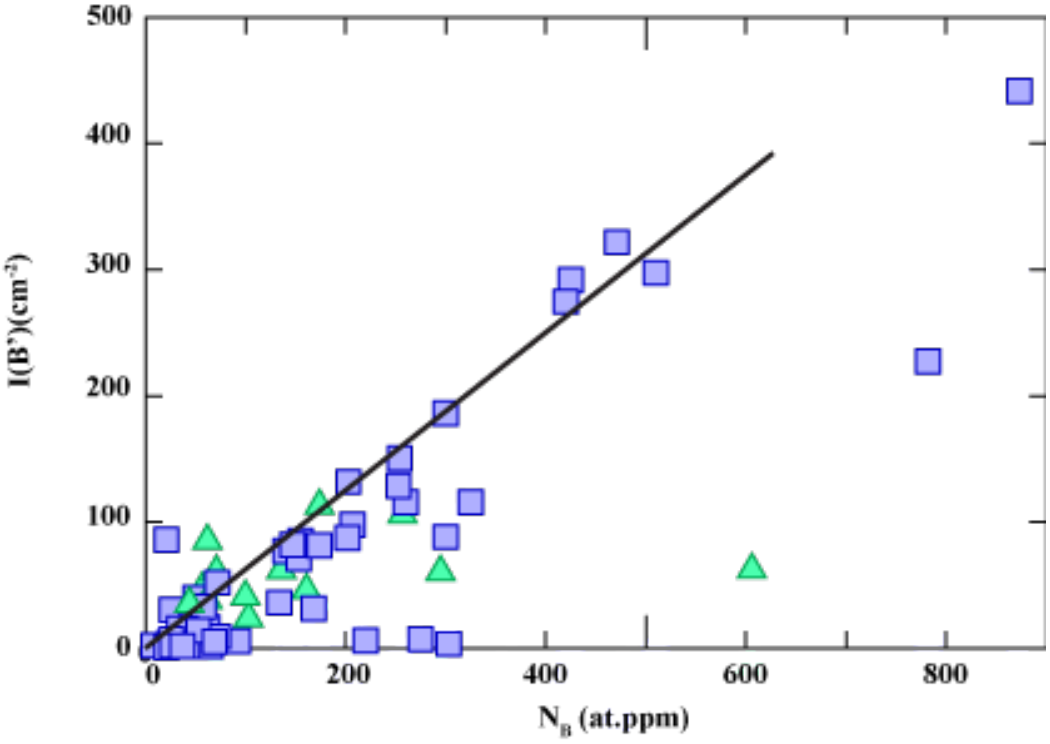


**Figure 2.9.** Platelet peak intensity (I(B')) versus abundance of nitrogen as B-center (at.ppm). The dashed line indicates the linear relationship between platelet intensity and B aggregates observed for 'normal' diamonds

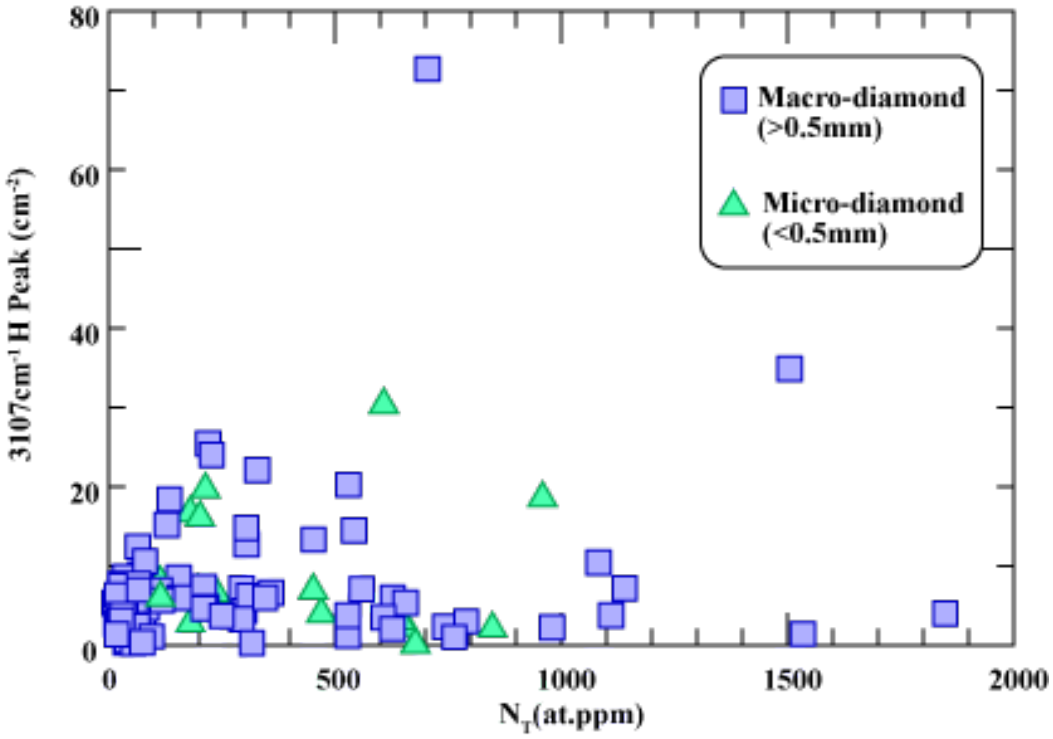


**Figure 2.10**. The relationship between the hydrogen related peak at 3107cm$^{-1}$ and the total nitrogen content ($N_T$) for diamonds from Artemisia

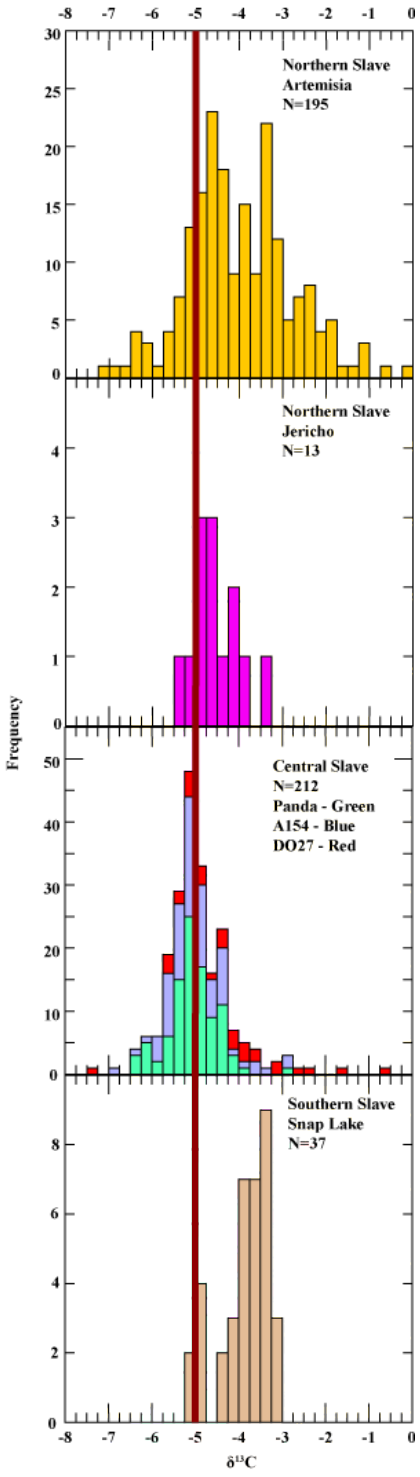


**Figure 2.11.** Carbon isotopic compositions of diamonds from the Slave Craton, ranging in $\delta^{13}C$ from -8‰ to 0‰. Red line denotes presumed mantle carbon isotopic composition (-5‰).

# Chapter 3

# General Discussion and Conclusions

The previous chapter provides a detailed description of the results of this geochemical study of diamonds from the Artemisia kimberlite. The purpose of this study was to investigate a possible co-genetic relationship of micro- and macro-diamonds, which is indicated by lognormal size frequency distributions encompassing micro- and macro-diamonds. From this study, some general conclusions can be drawn regarding the geochemical characteristics of diamonds from Artemisia and the nature of the genetic relationship of micro- and macro-diamond.

## 3.1 Diamonds from Artemisia Kimberlite

The carbon isotopic composition of diamonds from the Artemisia kimberlite ranges in values from -24.5 to +1.6‰. While the paragenesis of Artemisia diamonds is unknown, the presence of isotopically light (< -10‰) and heavy (> +0‰) carbon compositions implies the presence of an eclogitic source component. This finding is consistent with the observation of a predominantly eclogitic source paragenesis for the only other studied diamond source in the Northern Slave, the Jericho kimberlite (De Stefano et al., 2009). The wide carbon isotopic range at Artemisia does not exclude the presence of peridotitic diamonds within the suite, as the majority of samples fall within the isotopic range between -5 to -3‰, which is common for both peridotitic and eclogitic diamonds worldwide.

Thermometric calculations, based on nitrogen concentration-aggregation characteristics and carried out for an assumed mantle residence time of 0.5Ga, indicate that Type Ia diamonds from Artemisia resided in the Earth's mantle at temperatures ranging from about 1000 to 1450°C (mean: ~1218 ±74°C). Assuming that such time averaged residence temperatures reflect steady state conditions, the corresponding depth range encompasses the entire diamond stable sub-continental

lithospheric mantle.

### 3.2 The Micro-/Macro-Diamond Relationship

In comparing diamond color for micro- and macro-diamonds from Artemisia, a conclusive result remained elusive, as an accurate determination of light body colours for micro-diamonds was not possible. In regards to crystal morphology, it is observed that a high proportion of resorbed (i.e., crystals with dodecahedral morphology) macro-diamonds exists. As this overall high degree of resorption is not observed for micro-diamonds, it can be concluded that little information can be gained from the assessment of micro-diamonds during early stage exploration with respect to predicting the quality of commercial sized stones for a potential deposit.

In comparing the $\delta^{13}C$ ranges for micro- and macro-diamonds from Artemisia, it is noted that there is a $^{13}C$ depleted component ($\delta^{13}C < -10‰$) which is exclusively observed among macro-diamonds, and that positive $\delta^{13}C$ values are restricted solely to the micro-diamond population. Both micro- and macro-diamonds display a similar bi-modal distribution in $\delta^{13}C$ values (modes in classes -5.0 to -4.5‰ and -3.5 to -3.0‰), though the main mode of the micro-diamonds is shifted to isotopically heavier values (-3.5 to -3.0‰) relative to macro-diamonds (main mode in class -5.0 to -4.5‰). Despite this minor shift in main mode and distinct signatures in extreme values, the bulk of micro and macro-diamonds is indistinguishable in terms of $\delta^{13}C$. The strongly $^{13}C$ depleted and $^{13}C$ enriched compositions observed in macro- and micro-diamonds, respectively, imply, however, that distinct diamond subpopulations are preferentially sampled and/or preserved in certain stone sizes.

Impurities in diamond such as hydrogen and nitrogen suggest significant geochemical differences exist between micro- and macro-diamonds. A hydrogen related absorption peak at $3107cm^{-1}$ is observed in the majority of the macro-

diamonds (94%) but in less than half of the micro-diamonds (40%). Also, the majority of micro-diamonds analysed are classified as Type II diamonds (N ≤10at. ppm) and, in general, have lower nitrogen contents than macro-diamonds.

Type Ia micro- and macro-diamonds show a similar range in nitrogen based mantle residence temperatures and share a common average of ~1218°C. While this implies that Type Ia micro- and macro-diamonds share a common mantle residence history, this conclusion cannot be extended to Type II diamonds.

In summary, the geochemistry of micro- and macro-diamonds from the Artemisia kimberlite suggests an overall similar origin. Distinct signatures observed with respect to $^{13}C$ enriched and depleted compositions and hydrogen and nitrogen content imply, however, that distinct subpopulations are preferentially sampled and/or preserved in certain size fractions. In regards to the evaluation of new kimberlite discoveries based on micro-diamond data this study implies that differences exist between the two size fractions with respect to both the resorption history and the exact mixture of diamonds from various sources and parageneses.

## References

De Stefano, A., Kopylova, M.G., Cartigny, P., Afanasiev, V. 2009. Diamonds and eclogites of the Jericho kimberlite (Northern Canada). Contributions to Mineralogy and Petrology 18: 295-315

# Appendix A

# Methodology

Appendix A

## A.1 Carbon Stable Isotope Analysis: Conventional Sealed Tube Combustion

The carbon stable isotopic composition ($\delta^{13}C$) of macro-diamonds was analyzed at the Stable Isotope Laboratory at the University of Alberta under the guidance of Dr. Karlis Muehlenbachs through conventional sealed tube combustion and subsequent analysis on a dual inlet mass spectrometer.

The macro-diamond samples were combusted in evacuated and sealed silica glass tubes. The resulting $CO_2$ gas was extracted and analyzed for isotopic composition by a Finnigan MAT 252 dual inlet mass spectrometer. Precision and accuracy of the mass spectrometer is ± 0.02‰. Inclusion free whole diamonds and fragments with masses ranging between 0.4-2.0 mg were filled into 6mm diameter silica glass tubes together with 1-2 g of 99.95% pure CuO. The silica tubes were evacuated until the extraction line pressure stabilized (approximately 30 minutes) and simultaneously sealed and removed from the vacuum line using a blow torch.

Filled and evacuated silica tubes were heated for at least 12 hours at ~ 980°C to convert the diamond samples into $CO_2$ gas, with CuO acting as an oxygen source. After heating, the silica tubes were allowed to cool for approximately 2 hours prior to extraction.

Extraction of the sample $CO_2$ was accomplished under vacuum. To achieve this, first the silica tubes were broken, allowing the sample gas to flow into the vacuum line. The extracted $CO_2$ was trapped with liquid nitrogen in sample tubes for transfer to the Finnigan MAT 252 dual inlet mass spectrometer.

$\delta^{13}C$ determination of the $CO_2$ with the mass spectrometer was completed in dual inlet mode. The $^{13}C/^{12}C$ ratio was obtained from measurements of the mass to charge ratios (m/z) consistent with 45(for $^{13}C^{16}O_2$) and 44 (for $^{12}C^{16}O_2$) and compared to known carbonate values to determine $\delta^{13}C$ composition relative to V-PDB (Vienna-Pee Dee Belemnite). As $^{12}C^{17}O$ interferes with $^{13}C^{16}O_2$, a $^{17}O$

correction was applied based on the abundance of $^{18}O$ in the analyses.

## A.2 Secondary Ion Mass Spectrometry (SIMS)

SIMS is a surface and near surface analytical method for in situ quantitative elemental analysis. The principle behind SIMS is sputtering. Sputtering involves the impact of high energy ions on the surface of a sample which results in the ejection of surficial material (Williams, 1985). The impact of the primary ions on the sample surface breaks bonds, resulting in a fraction of the sputtered material to become ionized. The sputtered secondary ions are interpreted to be representative of the original composition of the sample (Asher, 1994).This method is extremely sensitive allowing for the analysis of isotopic ratios and trace element abundances for small volume samples. SIMS, therefore, is ideal for determining the carbon stable isotopic composition and nitrogen concentrations of micro-diamonds. For this project, SIMS analyses were conducted on instruments equipped with multi-collectors, allowing all isotopes of interest (in this case $^{12}C$ and $^{13}C$) to be measured simultaneously, resulting in improved analytical precision.

The $\delta^{13}C$ of a subset of micro-diamonds (71) were analyzed using (SIMS) at the Edinburgh Ion Microprobe Facility (EIMF) at the University of Edinburgh under the supervision of Dr. John Craven. A second subset of micro-diamonds and diamond fragments (42) were analyzed for $\delta^{13}C$ at the Canadian Centre for Isotopic Microanalysis (CCIM) at the University of Alberta under the supervision of Dr. Richard Stern. At both facilities, nitrogen concentrations were also determined by SIMS. Analytical parameters used at both facilities are outlined in Table A.1.

### A.2.1. Principles of Analysis by SIMS

A beam of cesium positive ions bombarded the surface of cleaned and gold coated (to ensure conductivity) samples. Sputtered secondary ions are accelerated through an electrostatic analyzer and mass spectrometer for chemical identification.

The electrostatic analyzer consists of a pair of cylindrical electrodes which produce an electrostatic field. The secondary ions enter the electrostatic analyzer through an energy window, which filters undesirable and interfering cluster molecules (produced during sputtering) from the system. The mass spectrometer utilizes large magnets to create a constant magnetic field to separate secondary ion species by mass for detection. Coupling an electrostatic analyzer with the mass spectrometer increases the mass resolution (ie. the ability to distinguish two peaks with similar mass to charge ratios) and, therefore, the sensitivity of analyses. Energy filtered and mass separated secondary ions are then counted by either a Faraday cup (e.g., for carbon isotopic analyses) or an electron multiplier (e.g., for nitrogen analyses at low nitrogen abundance).

Quantitative analysis of materials using SIMS requires the use of standards because of matrix effects; Matrix effects cause variability of ion yields in dependence of the composition of the sample surface. Ion yields of different elements in the same matrix or of the same element in different matrices can vary. Matrix effects inhibit fully quantitative analyses without the use of well characterized standards (Williams, 1985; Asher, 1994) with homogeneous major-element compositions similar to the unknown sample (Hinton, 1990; Fitzsimons et al., 2000). Here, synthetic diamond standards were applied to compensate for matrix effects and to quantitatively determine carbon isotopic compositions and nitrogen concentrations of the micro-diamonds.

The precision of SIMS analyses can be approximated based on counting statistics. For extremely long counting times, the precision of SIMS stable isotope analyses is comparable to conventional analysis by gas-source mass spectrometry (Fitzsimons et al., 2000). Additionally, the precision of SIMS analyses is dependent on consistency of the ion microprobe ("instrumental drift"). Frequent analyzes of the

diamond standards were completed during analytical sessions to monitor instrument drift, to which appropriate corrections (via regression) were then applied.

### A.2.2. Determination of Carbon Isotopic Composition and Nitrogen Abundances from Secondary Ion Count Intensities

Carbon isotopic compositions ($\delta^{13}C$) were determined using the ratios of the $^{13}C$ and $^{12}C$ counts of the unknown diamond sample and the synthetic diamond standard using the equation:

$$\delta^{13}C \text{ (sample)} = (((^{13}C/^{12}C) \text{ s}/ (^{13}C/^{12}C) \text{ std}) \times \delta^{13}C(\text{std})$$

Where: $\delta^{13}C$ (sample) – the carbon isotopic composition of the diamond to be determined
$(^{13}C/^{12}C)$ s – the $^{13}C/^{12}C$ count ratio of the unknown diamond sample
$(^{13}C/^{12}C)$ std – the average $^{13}C/^{12}C$ count ratio of synthetic diamond standard (for that day)
$\delta^{13}C$ (std) – the known carbon isotopic composition of the diamond standard

The nitrogen concentrations (wt.ppm) of the diamonds were calculated, from the $^{14}N^{12}C/^{13}C_2$ count ratio of the analyses, using the equation:

$$\text{N (wt.ppm) sample} = (\text{N(wt.ppm)std} / (\text{N/C}) \text{ std}) \times (\text{N/C})\text{sample}$$

Where: N (wt.ppm) sample = nitrogen concentration of unknown sample
N (wt.ppm) std = nitrogen concentration of known diamond standard
(N/C) std = $^{14}N^{12}C/^{13}C_2$ count ratio of known diamond standard (for that day)
(N/C) sample = $^{14}N^{12}C/^{13}C_2$ count ratio of unknown diamond sample

Conversion of nitrogen concentration from weight ppm (wt.ppm) to atomic ppm (at.ppm) used the same conversion factor as Thomassot et al. (2007), such that:

$$N\ (at.ppm) = 0.856(N\ (wt.ppm))$$

### A.2.3. General Summary of Sample Preparation and SIMS Analyzes

#### A.2.3.1. Edinburgh Ion Microprobe Facility (EIMF)

Analyses at the EIMF used a Cameca IMS 1270 ion microprobe. Whole diamonds, cleaned in petroleum ether in an ultra-sonic bath for 15 minutes, were pressed into indium to expose naturally flat diamond faces (octahedral growth planes). The sample mounts were coated with a thin gold film prior to analysis to ensure electrical conductivity and thereby to prevent charging of the sample surface.

For $\delta^{13}C$ analyses, after 60s of pre-sputtering to remove the gold film, secondary ions were collected in 20 cycles of 5 seconds each in multi-collection mode using Faraday cups. A primary beam <20μm in diameter with 20kV impact energy and mass resolution of ~2400 was used. Synthetic diamond external standards with known carbon isotopic compositions were used to determine the sample carbon compositions (Whopper ~ -5.00‰; Synal ~ -23.92‰; TS ~ -22.73‰) relative to V-PDB. The internal precision is about ± 0.4‰ (2 sigma).

The nitrogen abundance of the diamonds was determined in mono-collection mode using an electron multiplier (EM). A 30μm rastered primary beam was used to reduce the count rate on the EM. Each analytical spot was pre-sputtered for 120s and analyzed for 40 cycles of 5seconds duration at a mass resolution of ~9500. The internal precision of the analyses is ±13%.

### A.2.3.2. Canadian Centre for Isotopic Microanalysis (CCIM)

Analyses of diamonds at CCIM used a Cameca 1280 ion microprobe. Diamond samples were mounted in epoxy pucks (≤5mm) and ground and polished with diamond embedded metal plates to a 6 μm finish to create a flat surface for analysis. The epoxy pucks were drilled out, embedded in indium, along with the synthetic diamond reference material, and coated with a thin film (20 nm) of gold.

The carbon isotopic composition of the diamond samples was determined in multi-collection mode using faraday cups for 5s per count cycle, with 20 cycles per analytical spot subsequent to 60s of pre-sputtering. Analyses were conducted using a cesium primary beam with an impact energy of 20kV and a mass resolution of ~2300. A synthetic diamond external standard with known carbon isotopic composition was used to determine the sample carbon compositions ($\delta^{13}C$ ~ -22.60‰) relative to V-PDB. The internal precision is about ± 0.2‰ (2sigma).

The nitrogen abundance of the diamonds was determined in multi-collection mode, either through the simultaneous collection with faraday cups or one faraday cup and one electron multiplier, for 5s per count cycle, with 10 cycles per analytical spot subsequent to 60s of pre-sputtering. The analyses were conducted with a mass resolution of ~7000, resulting in an estimated uncertainty of ±5%.

## A.3. Fourier Transform Infrared (FTIR) Spectrometry

Nitrogen characteristics (concentration and aggregation state), presence of hydrogen impurities and intensity of platelet defects was determined for the Artemisia diamond samples using Fourier Transform Infrared (FTIR) spectroscopy in the De Beers Laboratory for Diamond Research at the University of Alberta using a Thermo Nicolet Nexus 470 FT-IR spectrometer coupled with a Continuum microscope with a KBr beam splitter.

The measurements were carried out on whole diamonds and fragments attached to the side of a glass slide with double sided adhesive tape. The instrument was purged with $H_2O$ and $CO_X$ free air to ensure stable background conditions. Using an aperture size of 50 x 50μm and operating in transmitted mode, IR spectra were collected in 200 cycles over the wave number range 650-4000$cm^{-1}$. Background measurements were taken at the beginning of each analytical session and repeated at regular intervals (every few hours).

Quantitative determination of nitrogen contents and aggregation states required a baseline correction and subsequent conversion of measured absorbance to absorption coefficient (i.e. normalization to a sample thickness of 1cm) which was achieved by normalizing the diamond related absorbance at 1995 $cm^{-1}$ to the established value of 11.94 $cm^{-1}$.

To determine the absorption coefficients for A- and B-centers, spectra were de-convoluted in the range 1000-1400$cm^{-1}$ using software provided by Dr. David Fisher (Research Laboratories of the Diamond Trading Company, Maidenhead, UK). Concentrations of nitrogen in A- and B-center aggregation was then determined by multiplying the respective absorption coefficients with conversion factors experimentally determined by Boyd et al. (1994) and Boyd et al. (1995).

## Appendix A

Hydrogen impurities and platelet defects of the diamonds were determined from normalized (to 1 cm sample thickness) spectra by measuring the peak height at 3107$cm^{-1}$ (hydrogen related peak) and the area under the platelet related absorption peak between 1358 and 1380$cm^{-1}$ relative to a base line.

## References

Asher, S.E. 1994. Secondary Ion Mass Spectrometry. In: Yacobi, B.G., Holt, D.B., Kazmerski, L.L. (eds.) Microanalysis of Solids, Plenum Press, New York, pp. 149-178

Boyd, S.R., Kiflawa, I., Woods, G.S. 1994. The relationship between infrared absorption and the A defect concentration in diamond. Philosophical Magazine Part B 69(6): 1149-1153

Boyd, S.R., Kiflawa, I. Woods, G.S. 1995. Infrared-absorption by the B-nitrogen aggregate in diamond. Philosophical Magazine Part B 72(3): 351-361

Fitzsimons, I.C.W., Harte, B., Clark, R.M. 2000. SIMS stable isotope measurement: counting statistics and analytical precision. Mineralogical Magazine 64(1): 59-83

Hinton, R.W. 1990. Ion microprobe trace-element analysis of silicates: measurement of multi- element glasses. Chemical Geology 83: 11-25

Thomassot, E., Cartigny, P., Harris, J.W., Viljoen, K.S. 2007. Methane-related diamond crystallization in the Earth's mantle: Stable isotope evidences from the single diamond bearing xenolith. Earth and Planetary Science Letters 257: 361-371

Williams, P. 1985. Secondary Ion Mass Spectrometry. Annual Review of Material Science 15: 517-548

**Table A.1.** Analytical conditions for Secondary Ion Mass Spectrometry (SIMS) analyses of carbon isotopic composition and nitrogen abundance of diamonds at the University of Alberta (CCIM) and the University of Edinburgh (EIMF)

| Analytical Parameter | EIMF | | CCIM | |
|---|---|---|---|---|
| | $\delta^{13}C$ (‰) | N (wt. ppm) | $\delta^{13}C$ (‰) | N (wt. ppm) |
| Primary Beam | $^{133}Cs^{+}$ | $^{133}Cs^{+}$ | $^{133}Cs^{+}$ | $^{133}Cs^{+}$ |
| Primary beam diameter | <20µm | rastered 30µm | 15 µm | 15 µm |
| Electron charge neutralization | No | No | No | No |
| Primary Beam Current | 7 nA | 6 nA | 3 nA | 1 nA |
| Primary Beam Impact Energy | 20 keV | 20 keV | 20 keV | 20 keV |
| Field Aperature | 4094 µm | 940 µm | 5000 µm | 2000 µm |
| Entrance Slit | 69 µm | 10 µm | 120 µm | 45 µm |
| Exit Slit (s) | 400 µm | 127 µm | 500 µm | 500 µm, 140 µm |
| Energy Window | 40eV | 40eV | 40eV | 40eV |
| Contrast Aperture | 400 µm | 400 µm | 400 µm | 400 µm |

**Table A.1.** cont.

| Analytical Parameter | EIMF | | CCIM | |
|---|---|---|---|---|
| | $\delta^{13}C$ (‰) | N (wt. ppm) | $\delta^{13}C$ (‰) | N (wt. ppm) |
| Image Magnification at FA | 200X | 100X | 100X | 100X |
| Pre-sputter | 60s | 120s | 60s | 60s |
| Seconday ions | $^{13}C^-$ and $^{12}C^-$ | $^{12}C^{13}C^-$ and $^{12}C^{14}N^-$ | $^{13}C^-$ and $^{12}C^-$ | $^{12}C^{12}C^-$ and $^{12}C^{14}N^-$ |
| Secondary extraction potential | 10kV | 10kV | 10kV | 10kV |
| Counting Mode | multi-collection simultaneous counting on Faraday cups | mono-collection on electron multiplier | multi-collection simulaneous counting on Faraday cups | multi-collection simulaneous counting on Faraday cups or Faraday + electron multiplier |

**Table A.1.** cont.

| Analytical Parameter | EIMF | | CCIM | |
|---|---|---|---|---|
| | $\delta^{13}C$ (‰) | N (wt. ppm) | $\delta^{13}C$ (‰) | N (wt. ppm) |
| Counting | 5s count time for both $^{13}C^-$ and $^{12}C^-$ for 20 cycles | 2s count time for both $^{12}C^{13}C$- and $^{14}N^{12}C$ for 40 cycles | 5s count time for both $^{13}C^-$ and $^{12}C^-$ for 20 cycles | 5s count time for both $^{12}C^{12}C^-$ and $^{12}C^{14}N^-$ for 10 cycles |
| Mass Resolution | ~2400 | ~ 9500 | $^{13}C^-$ ~2300, with offset center to low mass | $^{12}C^{14}N^-$ ~ 7000 |

# Appendix B

## Analytical Data for Diamonds from the Artemisia Kimberlite

## Tables

**Table B.1.** Carbon isotopes and nitrogen content (total analyses) using secondary ion mass spectrometry (SIMS)

| Sample | $\delta^{13}C$ (‰) | $N_T$ (wt.ppm) | $N_T$ (at.ppm) | Sample | $\delta^{13}C$ (‰) | $N_T$ (wt.ppm) | $N_T$ (at.ppm) |
|---|---|---|---|---|---|---|---|
| Art-13/1* | -2.61 | | | Art-29/2* | -2.06 | | |
| Art-13/2* | -2.26 | | | Art-29/3* | -2.54 | | |
| Art-14/1 | -4.04 | 89 | 76 | Art-30/1 | -4.64 | 18 | 15 |
| Art-14/2 | -3.84 | 85 | 73 | Art-30/2 | -4.62 | | |
| Art-14/3 | -3.86 | | | Art-30/3 | -4.56 | | |
| Art-14/4 | -4.14 | | | Art-30/4 | -4.50 | | |
| Art-14/5 | -4.13 | | | Art-30/5 | -4.51 | | |
| Art-15/1* | -3.34 | | | Art-30/6 | -4.66 | | |
| Art-15/2* | -3.09 | | | Art-30/7 | -4.66 | | |
| Art-15/3* | -3.41 | | | Art-34/1 | -2.38 | 23 | 20 |
| Art-16/1 | -4.34 | 5 | 4 | Art-34/2 | -2.32 | 21 | 18 |
| Art-16/2 | -4.09 | 2 | 2 | Art-34/3 | -2.46 | | |
| Art-16/3 | -4.08 | | | Art-34/4 | -2.49 | | |
| Art-21/1 | -4.83 | 141 | 121 | Art-34/5 | -2.33 | | |
| Art-21/2 | -4.73 | 313 | 268 | Art-34/6* | -1.26 | | |
| Art-21/3 | -4.76 | 477 | 408 | Art-34/7* | -1.52 | | |
| Art-21/4 | -4.81 | 587 | 503 | Art-34/8* | -1.30 | | |
| Art-21/5 | -5.04 | 362 | 310 | Art-34/9* | -1.34 | | |
| Art-21/6 | | 480 | 411 | Art-34/10* | -1.32 | | |
| Art-22/1* | -4.63 | | | Art-34/11* | -1.37 | | |
| Art-22/2* | -4.32 | | | Art-36/1 | -4.04 | 17 | 15 |
| Art-23/1* | -2.85 | | | Art-36/2 | -3.70 | 16 | 14 |
| Art-23/2* | -2.36 | | | Art-36/3 | -4.07 | | |
| Art-25/1* | -3.35 | | | Art-36/4 | -4.28 | | |
| Art-25/2* | -3.53 | | | Art-36/5 | -4.09 | | |
| Art-261* | -3.81 | | | Art-37/1* | -3.70 | | |
| Art-26/2* | -3.84 | | | Art-37/2* | -3.07 | | |
| Art-27/1 | -3.21 | 898 | 769 | Art-40/1* | -3.72 | 105 | 90 |
| Art-27/2 | -3.26 | 917 | 785 | Art-40/2* | -3.82 | 103 | 88 |
| Art-27/3 | -3.24 | | | Art-41/1* | 0.64 | | |
| Art-27/4 | -3.28 | | | Art-41/2* | 0.36 | | |
| Art-27/5 | -3.20 | | | Art-41/3* | 0.45 | | |
| Art-28/1 | -3.04 | 6 | 5 | Art-41/4* | -0.19 | | |
| Art-28/2 | -2.98 | | | Art-41/5* | 0.19 | | |
| Art-28/3 | -2.97 | | | Art-41/6* | 0.07 | | |
| Art-29/1* | -2.10 | | | Art-42/1* | -4.26 | | |

**Table B.1. cont.**

| Sample | $\delta^{13}C$ (‰) | $N_T$ (wt.ppm) | $N_T$ (at.ppm) | Sample | $\delta^{13}C$ (‰) | $N_T$ (wt.ppm) | $N_T$ (at.ppm) |
|---|---|---|---|---|---|---|---|
| Art-42/2* | -2.11 | | | Art-60/1* | -1.27 | 24 | 21 |
| Art-42/3* | -4.12 | 868 | 743 | Art-60/2* | -0.72 | | |
| Art-42/4* | -3.98 | 160 | 137 | Art-60/3* | -1.65 | 77 | 66 |
| Art-42/5* | -2.22 | | | Art-62/1* | 1.06 | | |
| Art-42/6* | -3.83 | 820 | 702 | Art-62/2* | 0.49 | | |
| Art-43/1* | -4.44 | 413 | 354 | Art-62/3* | 0.15 | 2 | 2 |
| Art-43/2* | -4.49 | 413 | 354 | Art-62/4* | -0.19 | | |
| Art-47/1* | 0.00 | | | Art-62/5* | 0.21 | 2 | 2 |
| Art-47/2* | 0.02 | | | Art-63/1 | -4.98 | 90 | 77 |
| Art-47/3* | -0.23 | | | Art-63/2 | -5.06 | | |
| Art-47/4* | 0.09 | | | Art-63/3 | -5.08 | | |
| Art-47/5* | 0.16 | | | Art-63/4 | -4.72 | | |
| Art-47/6* | -0.04 | | | Art-64/1* | -2.45 | 11 | 9 |
| Art-48/1 | -3.03 | 1 | 1 | Art-64/2* | -1.98 | 7 | 6 |
| Art-48/2 | -3.05 | 4 | 3 | Art-65/1* | -2.84 | 21 | 18 |
| Art-48/3 | -2.93 | | | Art-65/2* | -2.32 | 3 | 3 |
| Art-49/1 | -3.48 | 48 | 41 | Art-66/1* | -3.34 | 10 | 9 |
| Art-49/2 | -3.36 | | | Art-66/2* | -3.40 | 6 | 5 |
| Art-49/3 | -3.30 | | | Art-66/3* | -3.32 | 10 | 9 |
| Art-50/1 | -4.48 | 2 | 2 | Art-67/1 | -0.31 | 12 | 10 |
| Art-50/2 | -4.33 | 1 | 1 | Art-67/2 | -0.57 | 19 | 16 |
| Art-50/3 | -4.50 | | | Art-67/3 | -0.65 | | |
| Art-51/1 | -5.15 | 526 | 450 | Art-67/4* | -2.55 | 40 | 34 |
| Art-51/2 | -4.98 | | | Art-68/1* | -4.07 | 52 | 45 |
| Art-51/3 | -5.10 | | | Art-68/2* | -4.28 | 37 | 32 |
| Art-52/1 | -3.90 | 21 | 18 | Art-69/1* | -2.77 | 20 | 17 |
| Art-52/2 | -3.75 | | | Art-69/2* | -2.65 | 18 | 15 |
| Art-52/3 | -3.74 | | | Art-70/1 | -2.66 | 509 | 436 |
| Art-54/1 | -2.94 | 104 | 89 | Art-70/2 | -2.51 | | |
| Art-54/2 | -3.01 | | | Art-70/3 | -2.00 | | |
| Art-54/3 | -4.09 | | | Art-71/1 | -5.37 | 498 | 426 |
| Art-55/1* | -1.42 | | | Art-71/2 | -5.18 | | |
| Art-55/2* | -1.50 | | | Art-71/3 | -5.38 | | |
| Art-56/1* | -3.16 | 14 | 12 | Art-71/4 | -5.00 | | |
| Art-56/2* | -3.22 | 1 | 1 | Art-72/1* | 0.05 | 20 | 17 |
| Art-58/1* | -4.45 | 908 | 777 | Art-72/2* | 0.31 | | |
| Art-58/2* | -4.37 | 891 | 763 | Art-72/3* | 0.22 | | |
| Art-59/1 | -4.58 | 23 | 20 | Art-72/4* | 0.28 | | |
| Art-59/2 | -4.47 | | | Art-72/5* | 0.16 | | |
| Art-59/3 | -4.41 | | | Art-72/6* | 0.20 | 1 | 1 |
| Art-59/4 | -4.00 | | | Art-73/1* | -3.19 | 8 | 7 |

**Table B.1. cont.**

| Sample | $\delta^{13}C$ (‰) | $N_T$ (wt.ppm) | $N_T$ (at.ppm) | Sample | $\delta^{13}C$ (‰) | $N_T$ (wt.ppm) | $N_T$ (at.ppm) |
|---|---|---|---|---|---|---|---|
| Art-73/2* | -3.11 | | | Art-95/2 | -4.59 | | |
| Art-74/1 | -4.42 | 892 | 764 | Art-95/3 | -4.83 | | |
| Art-74/2 | -4.38 | 830 | 711 | Art-96/1 | -4.47 | 66 | 57 |
| Art-74/3 | -4.38 | | | Art-96/2 | -4.56 | | |
| Art-74/4 | -4.43 | | | Art-96/3 | -4.61 | | |
| Art-74/5* | -4.22 | | | Art-98/1 | -4.62 | 570 | 488 |
| Art-75/1* | -2.69 | | | Art-98/2 | -4.61 | 529 | 453 |
| Art-75/2* | -2.86 | | | Art-98/3 | -4.63 | | |
| Art-76/1* | -2.40 | 320 | 274 | Art-98/4* | -2.58 | | |
| Art-76/2* | -2.24 | 318 | 272 | Art-98/5* | -2.48 | | |
| Art-77/1* | -4.81 | 288 | 247 | Art-110/1 | -3.74 | 9 | 8 |
| Art-77/2* | -4.72 | 430 | 368 | Art-110/2 | -3.80 | | |
| Art-80/1* | -8.39 | | | Art-110/3 | -4.04 | | |
| Art-80/2* | -10.00 | | | Art-112/1 | -3.84 | 14 | 12 |
| Art-80/3* | -8.74 | | | Art-112/2 | -3.92 | | |
| Art-80/4* | -9.98 | | | Art-112/3 | -4.23 | | |
| Art-80/5* | -10.04 | | | Art-114/1 | -3.89 | 19 | 16 |
| Art-80/6* | -8.75 | | | Art-114/2 | -3.93 | | |
| Art-81/1 | -5.19 | 27 | 23 | Art-114/3 | -3.79 | | |
| Art-81/2 | -5.36 | | | Art-120/1 | -4.82 | 49 | 42 |
| Art-81/3 | -5.37 | | | Art-120/2 | -4.52 | | |
| Art-82/1* | -2.97 | | | Art-120/3 | -4.44 | | |
| Art-82/2* | -3.13 | | | Art-123/1 | -3.47 | 10 | 9 |
| Art-83/1* | -4.52 | 547 | 468 | Art-123/2 | -3.54 | | |
| Art-83/2* | -4.35 | 591 | 506 | Art-123/3 | -3.12 | | |
| Art-84/1 | -3.68 | 16 | 14 | Art-124/1 | -3.86 | 17 | 15 |
| Art-84/2 | -3.62 | 17 | 15 | Art-124/2 | -3.88 | 20 | 17 |
| Art-84/3 | -3.44 | 17 | 15 | Art-124/3 | -3.89 | | |
| Art-84/4 | -3.58 | | | Art-124/4 | -3.77 | | |
| Art-84/5 | -3.51 | | | Art-124/5 | -3.98 | | |
| Art-84/6* | -3.46 | | | Art-125/1 | -3.38 | 14 | 12 |
| Art-84/7* | -3.48 | | | Art-125/2 | -3.55 | 13 | 11 |
| Art-92/1 | -2.80 | 453 | 388 | Art-125/3 | -3.65 | | |
| Art-92/2 | -3.00 | 473 | 405 | Art-125/4 | -3.65 | | |
| Art-92/3 | -4.23 | | | Art-127/1 | -3.57 | 23 | 20 |
| Art-94/1 | -3.97 | 23 | 20 | Art-127/2 | -3.58 | 24 | 21 |
| Art-94/2 | -11.15 | 25 | 21 | Art-127/3 | -3.68 | 26 | 22 |
| Art-94/3 | -4.38 | | | Art-127/4 | -3.66 | | |
| Art-94/4 | -3.75 | | | Art-127/5* | -3.09 | | |
| Art-94/5 | -3.69 | | | Art-127/6* | -3.12 | | |
| Art-95/1 | -4.69 | 55 | 47 | Art-127/7* | -3.10 | 22 | 19 |

**Table B.1. cont.**

| Sample | $\delta^{13}C$ (‰) | $N_T$ (wt.ppm) | $N_T$ (at.ppm) | Sample | $\delta^{13}C$ (‰) | $N_T$ (wt.ppm) | $N_T$ (at.ppm) |
|---|---|---|---|---|---|---|---|
| Art-130/1 | -3.68 | 11 | 9 | ArtB/1 | -4.28 | 12 | 10 |
| Art-130/2 | -3.44 | 5 | 4 | ArtB/2 | -4.65 | | |
| Art-130/3 | -3.56 | | | ArtB/3 | -4.53 | | |
| Art-130/4 | -3.53 | | | ArtC/1 | -4.69 | 35 | 30 |
| Art-136/1 | -5.18 | 37 | 32 | ArtC/2 | -4.77 | | |
| Art-136/2 | -4.88 | | | ArtD/1 | -4.38 | 262 | 224 |
| Art-136/3 | -4.65 | | | ArtD/2 | -4.21 | 305 | 261 |
| Art-136/4 | -4.98 | | | ArtD/3 | -4.05 | | |
| Art-138/1* | -4.00 | 53 | 45 | ArtE/1 | -3.20 | 17 | 15 |
| Art-138/2* | -3.93 | 65 | 56 | ArtE/2 | -3.10 | 18 | 15 |
| Art-138/3* | -3.89 | 48 | 41 | ArtE/3 | -3.13 | | |
| Art-139/1* | -4.62 | 1022 | 875 | ArtF/1 | -3.20 | | |
| Art-139/2* | -4.34 | 102 | 87 | ArtF/2 | -6.22 | | |
| Art-139/3* | -4.09 | 192 | 164 | ArtF/3 | -3.17 | | |
| Art-139/4* | | 234 | 200 | ArtF/4 | -3.35 | | |
| Art-143/1* | -4.78 | 808 | 692 | ArtG/1 | -3.77 | 14 | 12 |
| Art-143/2* | -4.81 | 475 | 407 | ArtH/1 | -4.53 | 276 | 236 |
| Art-143/3* | -4.75 | 541 | 463 | ArtH/2 | -4.56 | 274 | 235 |
| Art-148/1* | -3.66 | | | ArtH/3 | -4.55 | 261 | 223 |
| Art-148/2* | -3.58 | | | ArtI/1 | -4.31 | 10 | 9 |
| Art-148/3* | -3.59 | | | ArtI/2 | -4.48 | 9 | 8 |
| Art-149/1* | -3.54 | 17 | 15 | ArtI/3 | -4.40 | | |
| Art-149/2* | -3.42 | 15 | 13 | ArtJ/1 | -2.44 | 3 | 3 |
| Art-149/3* | -4.24 | | | ArtJ/2 | -2.62 | | |
| Art-246/1 | -2.85 | 29 | 25 | ArtJ/3 | -2.79 | | |
| Art-246/2 | -1.56 | 74 | 63 | ArtK/1 | -3.55 | 2 | 2 |
| Art-246/3 | -3.43 | | | ArtK/2 | -3.35 | | |
| Art-247/1 | -3.30 | 6 | 5 | ArtK/3 | -3.42 | | |
| Art-247/2 | -3.47 | | | ArtL/1 | -3.88 | | |
| Art-247/3 | -3.49 | | | ArtL/2 | -3.82 | | |
| ArtA/1 | 2.59 | 1 | 1 | ArtM/AF/1 | -2.73 | 23 | 20 |
| ArtA/2 | 1.37 | 1 | 1 | ArtM/AF/2 | -2.36 | | |
| ArtA/3 | 0.94 | 22 | 19 | ArtM/AF/3 | -2.15 | | |
| ArtAA/1 | -3.37 | 268 | 229 | ArtM/AF/4 | -2.30 | 38 | 33 |
| ArtAA/2 | -3.30 | | | ArtM/AF/5 | -2.57 | 36 | 31 |
| ArtAB/1 | -5.32 | | | ArtN/1 | -3.20 | | |
| ArtAC/1 | -2.66 | | | ArtN/2 | -3.39 | | |
| ArtAC/2 | -2.73 | | | ArtO/1 | -3.33 | | |
| ArtAD/1 | -2.62 | | | ArtP/1 | -3.85 | 7 | 6 |
| ArtAE/1 | -1.37 | | | ArtP/2 | -3.57 | | |
| ArtAE/2 | -2.26 | | | ArtP/3 | -4.04 | | |

**Table B.1. cont.**

| Sample | $\delta^{13}C$ (‰) | $N_T$ (wt.ppm) | $N_T$ (at.ppm) | Sample | $\delta^{13}C$ (‰) | $N_T$ (wt.ppm) | $N_T$ (at.ppm) |
|---|---|---|---|---|---|---|---|
| ArtQ/1 | -3.28 | | | ArtV/1 | -1.83 | | |
| ArtQ/2 | -3.57 | | | ArtV/2 | -1.67 | | |
| ArtR/S/1 | -2.84 | 33 | 28 | ArtV/3 | -1.76 | | |
| ArtR/S/2 | -3.15 | | | ArtW/1 | -4.67 | 26 | 22 |
| ArtR/S/3 | -3.31 | 34 | 29 | ArtW/2 | -4.69 | 25 | 21 |
| ArtR/S/4 | -3.53 | | | ArtW/3 | -4.79 | | |
| ArtT/1 | -4.36 | 173 | 148 | ArtX/1 | -4.57 | | |
| ArtT/2 | -4.79 | 38 | 33 | ArtY/1 | -4.63 | | |
| ArtT/3 | -4.63 | | | ArtY/2 | -4.53 | | |
| ArtU/1 | -9.24 | 20 | 17 | ArtZ/1 | -3.20 | 12 | 10 |
| ArtU/2 | -9.29 | | | ArtZ/2 | -3.29 | | |
| ArtU/3 | -9.03 | | | ArtZ/3 | -3.06 | | |

* analyses completed at the University of Alberta

**Table B.2.** Masses of diamonds (whole crystals or fragments) combusted during conventional carbon isotopic analysis

| Sample | Mass (mg) | $\delta^{13}C$ (‰) | Sample | Mass (mg) | $\delta^{13}C$ (%) | Sample | Mass (mg) | $\delta^{13}C$ (%) |
|---|---|---|---|---|---|---|---|---|
| Art-2 | 1.1 | -5.99 | Art-175 | | -4.73 | Art-215 | 0.8 | -4.52 |
| Art-3 | 0.8 | -6.39 | Art-176 | 0.5 | -21.31 | Art-216 | | -3.11 |
| Art-4 | 0.4 | -4.85 | Art-177 | | -4.18 | Art-217 | 0.4 | -5.33 |
| Art-5 | 1.3 | -5.16 | Art-178 | 0.7 | -5.45 | Art-218 | 0.7 | -1.92 |
| Art-6 | 0.8 | -5.44 | Art-179 | | -3.69 | Art-220 | 1.0 | -3.76 |
| Art-8 | 1.0 | -6.72 | Art-180 | 0.4 | -4.95 | Art-221 | | -4.97 |
| Art-11 | 0.7 | -4.30 | Art-182 | 0.9 | -5.07 | Art-222 | 0.6 | -5.00 |
| Art-138 | 0.4 | -7.11 | Art-183 | 0.5 | -2.45 | Art-223 | | -4.18 |
| Art-139 | 0.5 | -4.64 | Art-184 | 1.1 | -4.64 | Art-224 | 0.7 | -5.25 |
| Art-142 | 1.4 | -2.06 | Art-186 | 2.0 | -3.89 | Art-225 | 0.5 | -4.42 |
| Art-143 | 0.5 | -5.04 | Art-188 | 1.4 | -2.82 | Art-226 | 0.6 | -4.43 |
| Art-144 | 0.4 | -24.50 | Art-189 | 0.9 | -1.94 | Art-227 | 0.5 | -5.10 |
| Art-146 | 0.6 | -0.16 | Art-190 | 0.8 | -1.76 | Art-228 | 0.7 | -4.34 |
| Art-147 | 1.1 | -4.46 | Art-191 | | -4.69 | Art-229 | 0.5 | -5.59 |
| Art-148 | 1.2 | -3.86 | Art-192 | | -4.23 | Art-230 | 2.0 | -5.70 |
| Art-149 | 0.4 | -2.46 | Art-193 | | -2.45 | Art-231 | | -2.83 |
| Art-150 | | -6.39 | Art-194 | | -3.08 | Art-232 | | -4.97 |
| Art-151 | 1.1 | -6.38 | Art-195 | 0.4 | -6.77 | Art-233 | 2.0 | -8.29 |
| Art-153 | 1.2 | -4.77 | Art-196 | 0.4 | -5.20 | Art-234 | 0.7 | -2.06 |
| Art-155 | 0.5 | -4.67 | Art-197 | 1.0 | -3.53 | Art-235 | 0.9 | -23.30 |
| Art-156 | 0.6 | -4.09 | Art-198 | 1.3 | -3.43 | Art-236 | 0.5 | -4.19 |
| Art-158 | 0.7 | -1.88 | Art-199 | 0.7 | -3.42 | Art-237 | 2.0 | -3.45 |
| Art-159 | 1.8 | -5.70 | Art-200 | 0.5 | -4.86 | Art-238 | 0.7 | -6.22 |
| Art-160 | 0.6 | -6.01 | Art-201 | 0.4 | -3.19 | Art-239 | 0.7 | -4.53 |
| Art-162 | 0.8 | -1.23 | Art-202 | 0.6 | -4.49 | Art-240 | 1.8 | -4.42 |
| Art-164 | 0.9 | -14.23 | Art-203 | 0.7 | -23.00 | Art-241 | 0.7 | -9.88 |
| Art-165 | 0.8 | -3.52 | Art-204 | 0.4 | -5.28 | Art-242 | 1.5 | -4.74 |
| Art-166 | 0.4 | -5.20 | Art-205 | 1.0 | -4.54 | Art-243 | 0.6 | -4.64 |
| Art-167 | 1.2 | -5.35 | Art-206 | | -4.66 | Art-244 | 1.2 | -6.18 |
| Art-168 | 0.9 | -5.17 | Art-207 | | -4.33 | Art-245 | 1.3 | -5.14 |
| Art-169 | | -4.98 | Art-208 | | -4.33 | Art-248 | 0.4 | -4.94 |
| Art-170 | | -3.40 | Art-209 | | -3.74 | Art-249 | 0.5 | -5.13 |
| Art-171 | | -3.23 | Art-210 | 0.7 | -3.72 | Art-252 | 0.5 | -1.18 |
| Art-172 | | -3.70 | Art-211 | | -3.13 | Art-253 | 1.1 | -3.39 |
| Art-173 | | -3.31 | Art-212 | | -5.17 | Art-255 | 2.0 | -4.89 |
| Art-174 | | -3.88 | Art-214 | | -4.97 | Art-256 | 2.0 | -5.53 |

## Figures

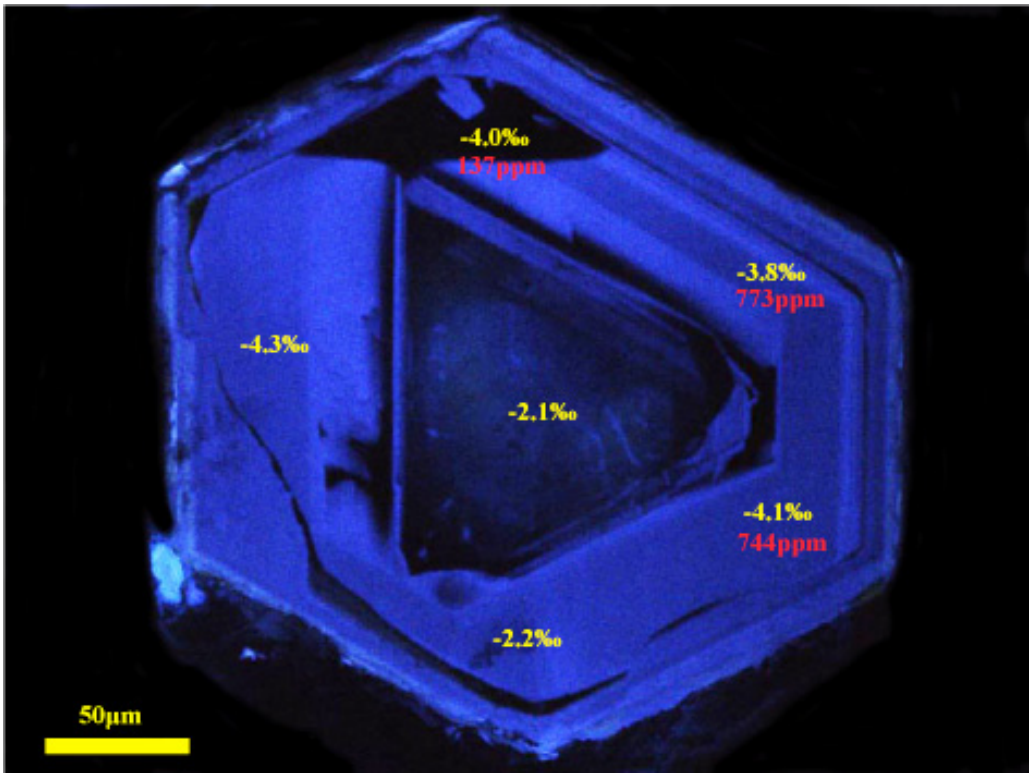


**Figure B.1.** CL image of cross section of Art-42 showing a diamond core over grown during a later growth event. Yellow and red text denotes carbon isotopic compositions and nitrogen abundances, respectively, corresponding to SIMS analyses conducted at CCIM.

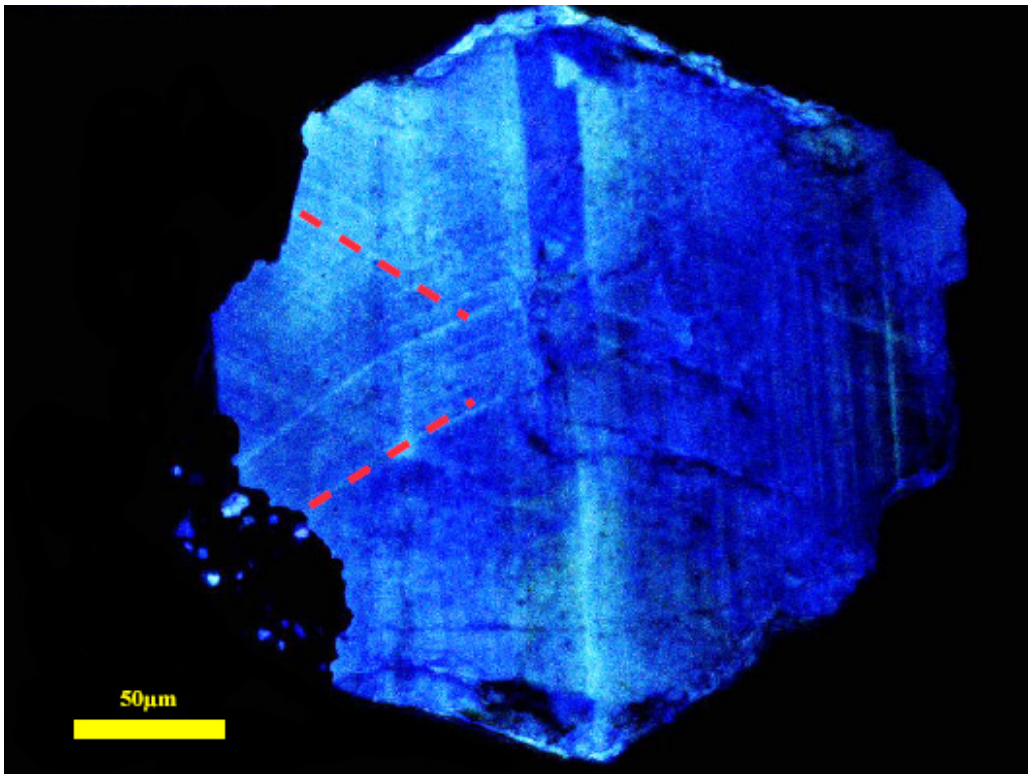


**Figure B.2.** CL image of Art-68 displaying two directions of plastic deformation (red dashed lines).

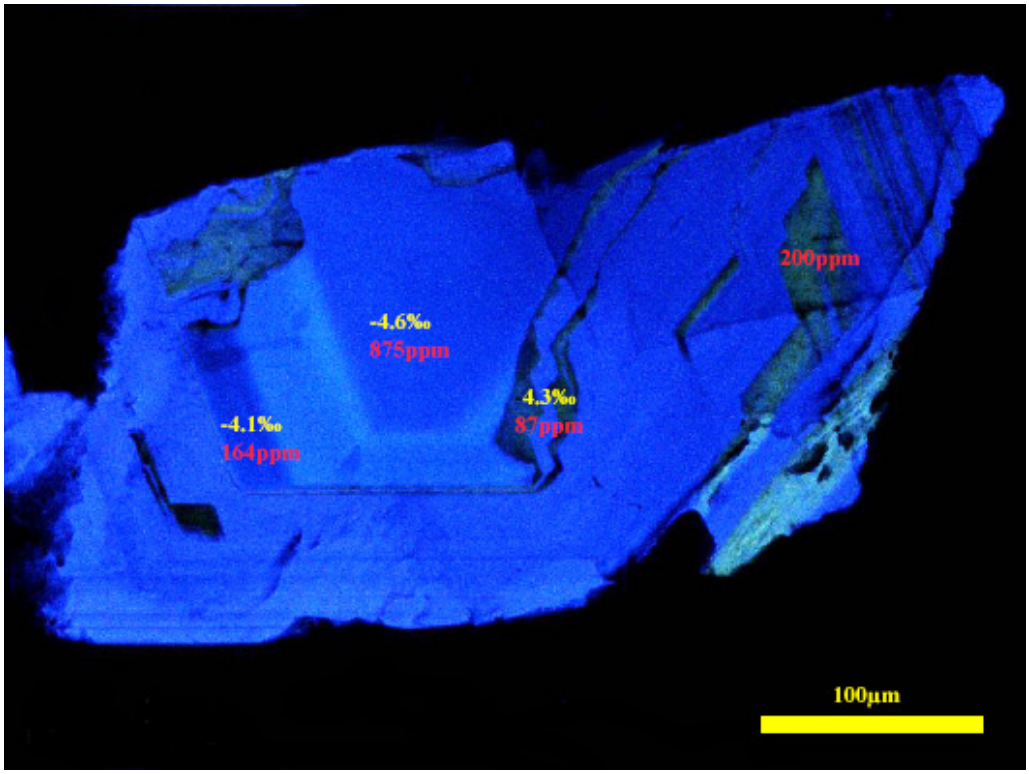


**Figure B.3**. CL image of a fragment of Art-139 displaying multiple episodes of diamond growth and resorption. Yellow and red text denote carbon isotopic compositions and nitrogen contents, respectively, corresponding to SIMS analyses conducted at CCIM.